https://doi.org/10.5194/se-2021-115
Preprint. Discussion started: 29 September 2021

Delamination in Tibet: Deriving constraints from the density of eclogite

Zhilin Ye [a,b], Dawei Fan [a,*], Bo Li [a,b], Qizhe Tang [c], Jingui Xu [d,*], Dongzhou Zhang [d], Wenge Zhou [a]

[a] *Key Laboratory of High-Temperature and High-Pressure Study of the Earth's Interior, Institute of Geochemistry, Chinese Academy of Sciences, Guiyang, Guizhou 550081, China*

[b] *University of Chinese Academy of Sciences, Beijing 100049, China*

[c] *School of Information Engineering, Huzhou University, Huzhou, Zhejiang 313000, China*

[d] *Hawaii Institute of Geophysics and Planetology, School of Ocean and Earth Science and Technology, University of Hawaii at Manoa, Honolulu, Hawaii 96822, USA*

* Corresponding authors.

E-mail addresses: fandawei@vip.gyig.ac.cn (D. Fan), xujingui@hawaii.edu (J. Xu)

Abstract

Tibet, which is characterized by collisional orogens, has undergone the process of delamination or convective removal. The lower crust and mantle lithosphere appear to have been removed through delamination during orogenic development. Numerical and analog experiments demonstrate that the metamorphic eclogitized oceanic subduction slab or lower crust may promote gravitational instability due to its increased density. The eclogitized oceanic subduction slab or crustal root is believed to be denser than the underlying mantle and tends to sink. However, the density of eclogite under high-pressure and high-temperature conditions and density differences from the surrounding mantle is not preciously constrained. Here, we offer new insights into the derivation of eclogite density with a single experiment to constrain delamination in Tibet. Using *in situ* synchrotron X-ray diffraction combined with diamond anvil cell, experiments focused on minerals

https://doi.org/10.5194/se-2021-115
Preprint. Discussion started: 29 September 2021

(garnet, omphacite, and epidote) of eclogite are conducted under simultaneous high-pressure and high-temperature conditions, which avoids systematic errors. Fitting the pressure-temperature-volume data with the third-order Birch-Murnaghan equation of state, the thermal equation of state (EoS) parameters, including the bulk modulus (K_{T0}), its pressure derivative (K_{T0}'), the temperature derivative ($(\partial K_T/\partial T)_P$), and the thermal expansion coefficient (α_0), are derived. The densities of rock-forming minerals and eclogite are modeled along with the geotherms of two types of delamination. The delamination processes of subduction slab breakoff and the removal of the eclogitized lower crust in Tibet are discussed. The Tibetan eclogite which containing 40-60 vol. % garnet and 37-64% degrees of eclogitization can promote the delamination of slab break-off in Tibet. Our results indicate that eclogite is a major controlling factor in the initiation of delamination. A high abundance of garnet, a high Fe-content, and a high degree of eclogitization are more conducive to instigating the delamination.

Keywords:

Eclogite, Equation of state, Single-crystal X-ray diffraction, Delamination, Tibet

1. Introduction

The evolution of orogenesis is characterized by lithospheric removal during rapid surface uplift, mantle upwelling, and postcollisional magmatism, particularly in the Central Andes (e.g. Ehlers and Poulsen, 2009; Schurr et al., 2006), Himalayas (e.g. Jiménez-Munt et al., 2008; Singh and Kumar, 2009), and Dabie orogen (e.g. He et al., 2011; Zhang et al., 2010).

It is widely accepted that delamination is the most important mechanism of lithospheric removal. Delamination is induced and accompanied by two major requisites: (a) the density

https://doi.org/10.5194/se-2021-115
Preprint. Discussion started: 29 September 2021

difference caused by the negative buoyancy of the delaminated lithosphere; and (b) the presence of a weak lower crust (lower viscosity) that exists between the strong upper crust and lithospheric mantle. Usually, two types of delamination are believed to occur in orogen development. The first is the conventional definition of delamination proposed by Bird (1978, 1979), which was used to interpret the geodynamic evolution of the Colorado Plateau. In this scenario, mantle lithosphere peels back from the overlying upper crust and is removed entirely, with the rising hot mantle filling the lithospheric removal zone (e.g. Göğüş and Ueda, 2018; Krystopowicz and Currie, 2013; Schott and Schmeling, 1998; Sobolev and Babeyko, 2005). A weak decoupling layer, i.e, the lower crust, is an essential condition in this delamination model, which may be affected by the rheological behavior of the hydration, thermal, and chemical characteristics of the lithosphere (e.g. Burov and Watts, 2006; Morency, 2004; Schott and Schmeling, 1998). In addition to conventional delamination, an alternative delamination mechanism is convective removal based on the Rayleigh-Taylor-type instability model (Houseman et al., 1981), namely, viscous “dripping”. This model postulates that there is sufficient perturbation in the lithospheric mantle, which is ascribed to the strong temperature-dependence of typical mantle rheology, without regard to a specific weak layer (e.g. Conrad and Molnar, 1999; Gorczyk et al., 2012; Houseman and McKenzie, 1982; Schott and Schmeling, 1998).

All previous studies attribute the gravitational instability process of lithospheric removal to the negative thermal buoyancy of the cold lithosphere (Conrad and Molnar, 1999; Houseman and McKenzie, 1982) or density contrast between asthenosphere and mantle lithosphere (Elkins-Tanton, 2007; Neil and Houseman, 1999). In any case, the density distribution with lithosphere pressure and temperature (*P-T*) conditions and chemical composition is of vital

https://doi.org/10.5194/se-2021-115
Preprint. Discussion started: 29 September 2021

importance to understanding the process of lithospheric removal.

The Tibetan Plateau is the most representative and prominent collisional orogens. Two types of delamination are proposed to proceed (e.g. Chung et al., 2005; Houseman et al., 1981; Molnar et al., 1993; Platt and England, 1994; Sun et al., 2020): lithospheric mantle removal and thickened eclogitized crust removal. The Neo-Tethyan oceanic subduction, India-Asia collision, and Indian continental subduction could be further considered responsible for the abnormal thinning of the mantle lithosphere under Tibet (Chung et al., 2005; DeCelles et al., 2011; Li et al., 2019; Ma et al., 2017; Xu et al., 2008; Zhao et al., 2020). The lithospheric removal event in Tibet corresponds to Neo-Tethyan oceanic slab break-off. The mechanism is primarily based on density contrasts between the denser mantle lithosphere and the lighter underlying mantle. Some models reveal that lithospheric removal is induced by the retreating high-density eclogitized lithosphere detached from overlying low-density crust (Faccenda et al., 2009; Li et al., 2016; Ueda et al., 2012). Other alternative models indicate that thickened eclogitized crust is a potential factor deriving lithospheric removal because the eclogitized crustal root is denser than the underlying mantle and tends to sink (Krystopowicz and Currie, 2013). Regardless of the above types of delamination, the density of eclogite is closely related to delamination. Therefore, Tibet provides an excellent opportunity to understand the role of eclogite density in the process of delamination.

An immense amount of concrete research has focused on the origin and appearance of lithospheric mantle removal from different angles, such as geophysical (Ren and Shen, 2008; Tilmann, 2003), geological (Chung et al., 2005; Molnar et al., 1993), petrological (Chung et al., 2005; Turner et al., 1993), numerical and analog experiments (Bajolet et al., 2012; Göğüş and Pysklywec, 2008; Morency, 2004; Valera et al., 2011). In particular, numerical and analog

https://doi.org/10.5194/se-2021-115
Preprint. Discussion started: 29 September 2021

experiments are used as prominent methods to simulate the dynamics of delamination (Göğüş and Ueda, 2018). Of these studies, the density behavior occurring during the delamination process has also been investigated intensively following thermodynamic (Duesterhoeft et al., 2012; Semprich et al., 2010), seismic/tomography (Li and Fang, 2017; Matchette-Downes et al., 2019), and numerical simulations (Gerya et al., 2004; Li et al., 2016; Sobolev and Babeyko, 2005). However, few studies have systematically illuminated the issue of delamination from the perspective of eclogite density. Here, we attempt to offer new insights into the derivation of rock density through the mineral physics method to constrain delamination in Tibet (Ye et al., 2021). Conducting a single experiment under high-pressure and high-temperature conditions, we obtain the equation of state (EoS) of the main minerals of eclogite with fewer systematic errors in the experiment. Furthermore, the newly derived EoS of the main minerals of eclogite, combined with the published EoSs of the main minerals of peridotite (Ye et al., 2021), geothermal lines, and collected eclogite mineral compositions, are further used to elucidate a density evolution model during the delamination process in Tibet. We argue that the EoSs of minerals could be used in a straightforward manner as new constraints on the construction of the density model. Using a simplistic calculation setup, in this study, this density evolution model will shed light on the possibility of delamination during the orogen process.

2. Geological background

The Tibetan Plateau is composed of four terranes from south to north: the Himalaya, Lhasa, Qiangtang, and Songpan-Ganzi terranes (Fig. 1). The birth of the Himalayas and Tibetan Plateau is a consequence of the Indo-Asian collision, which began in the early Cenozoic (Hodges et al.,

https://doi.org/10.5194/se-2021-115
Preprint. Discussion started: 29 September 2021

Solid Earth Discussions

2001; Rowley, 1998; Wang et al., 2008). The Neo-Tethyan oceanic slab is proposed to have detached from the Indian lithosphere, and the onset of the Indo-Asian collision (DeCelles et al., 2002; Kohn and Parkinson, 2002) particularly occurred in the lower part of the Indian and Lhasa lithospheres. The tectonic evolutionary history of the Lhasa terrane and Tethys Himalayas is essential for revealing the origin of the Himalayan-Tibetan orogen. The subducting Neo-Tethyan slab was thrust into southern Tibet approximately 70-65 Ma (Fig. 1b). With the closure of the Neo Tethyan Ocean, the India-Asia continent collision caused compressional deformation in southern Tibet (Ding et al., 2003), and a series of collision breakoff events were delineated spanning from 65 Ma to 42 Ma (Chung et al., 2005, 2009; Lee et al., 2009; Leech et al., 2005; Ma et al., 2014; Zhu et al., 2011, 2015). During this period, the Indian continental lithosphere might have dragged down to deeper depths during subduction (Chemenda et al., 2000). Meanwhile, slab rollback accompanied by the southward migration of asthenospheric convection in Tibet changed the thermal structure of the mantle wedge. The breakoff of the oceanic Neo-Tethyan slab from the more buoyant Indian continental lithosphere indicated by the eruption of early Eocene Linzizong volcanic rocks in the Gangdese arc or the cessation of Gangdese arc magmatism occurred at ~45 Ma (DeCelles et al., 2002), which opened a channel for the upwelling asthenosphere (Chung et al., 2009; Ma et al., 2014; Zhu et al., 2015). Additionally, geophysical evidence of longitudinal wave (V_P) tomography is interpreted for the north-dipping high-speed anomaly, which is ascribed to the deep Indian mantle lithosphere (Li et al., 2008; Liang et al., 2016; Tilmann, 2003). Subsequently, the subduction of the Indian continental margin continues at a low subduction angle beneath the Lhasa terrane (Guillot et al., 2008).

In addition, 25 Ma to 0 Ma is another period considered to contain either the occurrence of slab

https://doi.org/10.5194/se-2021-115
Preprint. Discussion started: 29 September 2021

breakoff (Jiang et al., 2012; Miller et al., 1999) or lithospheric mantle removal following slab breakoff (Chung et al., 2005; Nomade et al., 2004). Previous studies suggested that the hotter asthenosphere considerably raised the geothermal conditions during this period (Chung et al., 2005; Hou et al., 2004; Williams et al., 2001). Magmatism of the ultrapotassic, shoshonitic, and calc-alkaline was widespread, which was potentially due to the partial melts of the metasomatized lithospheric mantle and eclogitized lower crust. An adopted model of convective lithospheric removal below Lhasa is widely followed (Miller et al., 1999; Molnar et al., 1993; Platt and England, 1994). The lithospheric removal-related mantle upwelling process has been supported by geological, geophysical, and petrological studies (Chung et al., 2005; Molnar et al., 1993; Ren and Shen, 2008; Turner et al., 1993).

Here, slab breakoff and convective lithospheric removal under Tibet are adopted as the background in this study to discuss the possibility of the delamination process.

3. Materials and methods

3.1 Starting material

Natural garnet, omphacite, and epidote samples are collected from eclogite in the Dabie-Sulu UHPM belt. The compositions of each mineral are determined to be $Prp_{21}Alm_{47}Grs_{31}Sps_{1}$ (Prp = pyrope, Alm = almandine, Grs = grossular, and Sps = spessartine) for garnet, $Quad_{48}Jd_{45}Ae_{7}$ (Quad = Ferrosilite + enstatite + wollastonite, Jd = jadeite, Ae = aegirine) for omphacite, and $Ca_{2.02}Fe_{0.75}Al_{2.32}Si_{0.16}[SiO_4][Si_2O_7]O(OH)$ for epidote. The compositions of garnet and omphacite are shown in Figure 2 and are within the range of natural mineral compositions of eclogite from Tibet. The chemical composition of representative epidote minerals in Tibet shows that the Fe

https://doi.org/10.5194/se-2021-115
Preprint. Discussion started: 29 September 2021

content of epidote exposed in eclogite is in the range of 0.13-0.25 ($X_{Fe}=Fe^{3+}/(Fe^{3+}+Al^{3+})$) (Huang et al., 2015; Li et al., 2017; Liu et al., 2016; Ma et al., 2017; Song et al., 2003; Weller et al., 2016; Yang et al., 2014), while the Fe content of epidote in this study is 0.24, which is within the Fe content range of natural epidote. The samples used in this study are representative of garnet, omphacite, and epidote minerals in natural eclogites from Tibet. The garnet, omphacite, and epidote with high-quality grains are separated from the eclogite specimens. The above three samples are crushed into 30×40 μm^2 chips with a single crystal thickness of 15 μm in our experiment.

3.2 Synchrotron X-ray diffraction

The high-pressure and high-temperature experiment is conducted by a BX90 externally-heated diamond anvil cell (EHDAC) with ±15° opening angles. The above three single crystals are loaded into the BX90 EHDAC equipped with a pair of 500 μm culet-size diamond anvils and WC seats (Figure S1). The rhenium (Re) gasket is pre-indented to a thickness of ~60 μm, and a cylindrical hole with a diameter of 360 μm is drilled as a sample chamber. Gold powder is also loaded as the pressure calibrant (Fei et al., 2007), and neon is loaded as the pressure transmitting medium through the GeoSoilEnviroCARS (GSECARS) gas loading system (Rivers et al., 2008). The quasi-hydrostatic condition in the sample chamber can be maintained up to ~20 GPa using the neon pressure transmitting medium (Finkelstein et al., 2017). On the other hand, high temperature can significantly decrease the deviatoric stress conditions in the sample chamber. Moreover, previous studies demonstrate that the deviatoric stress disappears at the temperatures of 650 K with neon as the pressure transmitting medium (Klotz et al., 2009; Meng et al., 1993). Therefore, the hydrostatic/quasi-hydrostatic conditions can be maintained within the *P-T* range of our

https://doi.org/10.5194/se-2021-115
Preprint. Discussion started: 29 September 2021

Solid Earth Discussions
Open Access

experiment (~700 K, 25 GPa). An automated pressure-driven membrane system is utilized to generate increasing pressure up to 25.6 GPa. High-temperature conditions up to 700 K are provided by the heating resistor. Setup details for the employed thermocouples and heaters can be found in our previous articles (Xu et al., 2019, 2020b; Ye et al., 2021).

In-situ synchrotron single-crystal X-ray diffraction (XRD) experiments were performed at experimental station 13-BM-C of the Advanced Photon Source, Argonne National Laboratory. The detailed experimental process and associated parameters can be seen in our previous studies (Xu et al., 2017, 2018, 2020a; Zhang et al., 2017a). The diffraction images and the lattice parameters were analyzed by the Bruker APEX3 software package (Dera et al., 2013). The specific unit-cell parameters of the above three samples at each *P*-*T* condition can be found in Table S1.

4 Results and discussions

4.1 EoS of main minerals for eclogite

The pressure-volume-temperature (*P*-*V*-*T*) data in this study are fitted by the high-temperature third-order Birch-Murnaghan-EoS (HT-BM3-EoS) (Birch, 1947) to obtain the thermal EoS parameters including the zero-pressure volume (V_{T0}), the isothermal bulk modulus (K_{T0}), and its pressure derivate (K_{T0}') with the following form:

$$P = (3/2)K_{T0}\left[\left(V_{T0}/V\right)^{7/3} - \left(V_{T0}/V\right)^{5/3}\right] \times \left\{1 + (3/4)\left(K_{T0}' - 4\right)\left[\left(V_{T0}/V\right)^{2/3} - 1\right]\right\} \quad (1)$$

where V_{T0} and K_{T0} at different isotherms are expressed by the following equations:

$$V_{T0} = V_0 \, exp \int_{300}^{T} \alpha_T \, \mathrm{d}T \quad (2)$$

$$K_{T0} = K_0 + \left(\partial K_T / \partial T\right)_P (T - 300) \quad (3)$$

where $(\partial K_T/\partial T)_P$ is the temperature derivative of the bulk modulus and α_T ($\alpha_T = \alpha_0 + \alpha_1 T + \alpha_2 T^{-2}$) is the thermal expansion coefficient at room pressure. Considering the limited high temperature experimental data in this study, we fixed α_1 and α_2 as 0 in the fitting.

The thermal EoS parameters are derived using the EoSFit program without any constraints at high-pressure and room-temperature and high-pressure and high-temperature conditions (Angel et al., 2014) and are shown in Table S2. Under ambient pressure and temperature conditions, the measured V_0 values of garnet, omphacite, and epidote are 1565.8 (4) Å^3, V_0 = 423.3 (4) Å^3, and V0 = 461.2 (2) Å^3, respectively. The fitting parameters under high-pressure and room-temperature yield K_{T0} = 172 (2) GPa, K_{T0}' = 3.6 (2) for garnet, K_{T0} = 124 (2) GPa, K_{T0}' = 3.7 (4) for omphacite, and K_{T0} = 122 (1) GPa, K_{T0}' = 2.5 (2) for epidote, respectively.

To evaluate the quality of BM3-EoS fitting in this study, the relationship between the Eulerian strain ($f_E = \left[\left(V_0 / V \right)^{2/3} - 1 \right]$) and the normalized pressure ($F_E = P / \left[3 f_E \left(2 f_E + 1 \right)^{5/2} \right]$) of the main minerals for eclogite is plotted in Figure S2. Linear fitting of the three sets of data exhibited a negative slope, indicating that the pressure derivative of the bulk modulus (K_{T0}') is less than 4, which is consistent with our BM3-EoS fittings. The intercept value was obtained by weighted linear regression of the data points, showing that $F_E(0)$=171 (2) GPa for garnet, $F_E(0)$=123 (2) for omphacite, and $F_E(0)$=122 (1) for epidote, respectively. The results are consistent with the fitted isothermal bulk modulus (K_{T0} = 172 (2) GPa for garnet, K_{T0} = 124 (2) GPa for omphacite, and K_{T0} = 122 (1) GPa for epidote, respectively) within the error range. Accordingly, the K_{T0} and K_{T0}' obtained by the BM3-EoS fitting are reasonable. Using the V_0 fixed at ambient conditions to fit HT-BM3-EoS, the available EoS parameters, K_{T0} = 171.4 (8) GPa, K_{T0}' = 3.5 (1), $(\partial K_T/\partial T)_P$ = -0.010 (3) GPaK^{-1}, and α_0 = 2.86 (9) ×10^{-5} K^{-1} for garnet; K_{T0} = 122 (2) GPa, K_{T0}' = 4.1 (3), $(\partial K_T/\partial T)_P$ = -0.025 (6) GPaK^{-1}, and α_0 = 4.7 (4) ×10^{-5} K^{-1} for omphacite; and K_{T0} = 122.7 (6) GPa, K_{T0}' = 2.49 (8), $(\partial K_T/\partial T)_P$ = -0.029 (2) GPaK^{-1}, and α_0 = 4.7 (1) ×10^{-5} K^{-1} for epidote are derived. The *P-V-T* data fitted through the HT-BM3-EoS model are shown in Figure 3.

4.2 Comparison with previous studies

4.2.1 Garnet

The thermal EoS parameters of garnet are obtained by fitting the *P-V-T* data to the BM3-EoS. We compare our results with those of previous studies (Arimoto et al., 2015; Gréaux and Yamada, 2014; Lu et al., 2013; Milani et al., 2015, 2017; Xu et al., 2019; Zou et al., 2012). The K_{T0} of end-member garnet, pyrope, almandine, grossular, and spessartine crystals is between 158 and 179 GPa, and the bulk modulus of almandine is the largest among the above (Table S3). From Table S3, it can be seen that the bulk modulus of powder XRD (Arimoto et al., 2015; Gréaux and Yamada, 2014; Pavese et al., 2001; Zou et al., 2012) are larger than those of single-crystal XRD (Milani et al., 2015, 2017) with the same composition. The K_{T0} of solid solution garnets (Beyer et al., 2021; Jiang et al., 2004; Lu et al., 2013; Xu et al., 2019) is also between 158 and 179 GPa mentioned above and will be affected by the end-member components. The K_{T0}=171.4 (8) GPa in this study is reasonable within this range. The obtained K_{T0}' =3.5 (1) in this study is slightly lower than that in previous studies. The Eulerian strain and the normalized pressure of the garnet shown in Figure S2(a) exhibit a negative slope, which indicating K_{T0}' is less than 4. Moreover, compared with the previous results, the obtained value of K_{T0}' in this study is within the error range (Supporting Information Text S1). However, there is no obvious correlation between the fitted K_{T0} and K_{T0}' for minerals of different compositions (Fig. S3); hence, the K_{T0} may not be precise when K_{T0}' is fixed. The value of $(\partial K_T/\partial T)_P$ = -0.010 (3) GPa/K in this study is close to that of Xu et al. (Xu et al., 2019) obtained through single-crystal XRD experiments, which reflects that the compositional effect on $(\partial K_T/\partial T)_P$ is minor, but $(\partial K_T/\partial T)_P$ is smaller than that of end-member

https://doi.org/10.5194/se-2021-115
Preprint. Discussion started: 29 September 2021

garnets obtained from energy-dispersive XRD experiments (Table S3). For the α_0, the andradite has the largest value (3.16 (2)×10^{-5} K^{-1}), and the grossular has the smallest value (2.09 (2)×10^{-5} K^{-1}) among the end-member garnets. The thermal expansion coefficient of $Prp_{21}Alm_{47}Grs_{31}Sps_1$ (2.86 (9)×10^{-5} K^{-1}) in this study is comparable with previous studies, but the influence of composition still needs to be considered (Supporting Information Text S2).

4.2.2 Omphacite

Many studies have focused on the thermoelastic properties of omphacite (Hao et al., 2019; Nishihara et al., 2003; Pandolfo et al., 2012b, 2012a; Xu et al., 2019; Zhang et al., 2016) (Table S3). Most of the results are obtained by the single-crystal XRD method, except for the result of Nishihara et al. (2003), which was obtained from powder XRD. K_{T0}' shows a higher value of 6.9 (12) in the study of Nishihara et al. (2003), while in others, K_{T0}' is between 4 and 5.7, and the result of K_{T0}' (4.1) in this study is exactly between the above values. Additionally, according to the results shown in Table S3, the bulk moduli of omphacite are in the range of 115-123 GPa. In the study of Xu et al. (2019), an increase in the iron content would decrease K_{T0}, and they also discussed the reasons for the discrepancy in K_{T0} in detail, such as the effective ionic radius, pressure transmitting medium, and experimental pressure range. Comparing our results with Xu et al. (2019), we conclude that the incorporation of Fe would reduce the bulk modulus. However, except for Fe content, there does not seem to be a significant correlation between the other components and the bulk modulus of omphacite. The α_0 of the Di-Jd solid solution is similar (2.64 (2) ×10^{-5} K^{-1}-2.8 (3)×10^{-5} K^{-1}) but less than that of $Quad_{48}Jd_{45}Ae_7$ (4.7 (4) ×10^{-5} K^{-1}) and $Quad_{53}Jd_{27}Ae_{20}$ (3.4 (4)×10^{-5} K^{-1}). It may be inferred that the Ae contents affect thermal expansion. The $(\partial K_T/\partial T)_P$ of $Quad_{48}Jd_{45}Ae_7$ in this study is -0.025 (6) GPa/K, which is larger than that of

https://doi.org/10.5194/se-2021-115
Preprint. Discussion started: 29 September 2021

$Quad_{57}Jd_{42}Ae_1$ and $Quad_{53}Jd_{27}Ae_{20}$ in the Xu et al. (2019) study.

4.2.3 Epidote

The thermal EoS parameters of epidote in this study are compared with those reported in previous studies (Fan et al., 2014; Gatta et al., 2011; Holland et al., 1996; Li et al., 2020; Qin et al., 2016) (Table S3). Although the bulk modulus appears to be related to the Fe^{3+} content, it does not show a good correlation. Increasing the content of Fe^{3+} can enhance the bulk modulus, but the result in Holland et al. (1996) shows an abnormally large value of 162 (4) GPa, which is much higher than the 111-133 GPa resulting from other studies. This may be attributed to the fixed K_{T0}' at 4 and powder XRD methods used in the study of Holland et al. (1996). Furthermore, the K_{T0}' obtained from powder XRD (Fan et al., 2014; Gatta et al., 2011) is also larger than that from single-crystal XRD (Qin et al., 2016). The possible reasons for these discrepancies are complicated. Li et al. (2020) conducted a detailed study on this topic. Previous studies on α_0 and $(\partial K_T/\partial T)_P$ of epidote are limited. The α_0 (4.7 (1) $\times 10^{-5}$ K^{-1}) in this study is similar to that of Gatta et al. (5.1 (2) $\times 10^{-5}$ K^{-1}) (Gatta et al., 2011) and slightly larger than that of Li et al. (3.8 (5) $\times 10^{-5}$ K^{-1}) (Li et al., 2020). In previous studies, only Li et al. (2020) derived the value of $(\partial K_T/\partial T)_P$ (-0.004 (1) GPa/K), which is much smaller than the absolute value produced in this study (-0.029 (2) GPa/K).

5 Implications

In the Himalayan-Tibetan system, lithospheric removal is proposed to occur in either the breakoff of the subducted slab of the Indian continental lithosphere (Chung et al., 2005; Liu et al., 2014; Turner et al., 1993; Zhao et al., 2009) or convective removal of the thickened lower part of the lithosphere (Husson et al., 2014; Miller et al., 1999; Tian et al., 2017; Zhang et al., 2017b). The

https://doi.org/10.5194/se-2021-115
Preprint. Discussion started: 29 September 2021

metamorphic eclogitization taking place in the subducted slab and the lowermost crust has been deduced as the possible cause of subducted slab break-off and the convective removal of the lower crust (Kind, 2002; Krystopowicz and Currie, 2013; Shi et al., 2015). Increased density in the eclogitized subducted slab and the lower crust will promote the above two lithospheric removal modes if the lower crust is weak enough for the negative buoyancy of the mantle lithosphere to be detached. Therefore, to better consider the role of eclogite density variations in the process of lithospheric removal, we model the density of minerals and eclogite aggregates along with the geotherms of Tibet and discuss the effects of the degree of eclogitization on lithospheric removal.

The eclogite chemical data collected in Tibet and examined in our study come from a great number of eclogite samples collected in previous studies (e.g. Chan et al., 2009; Liu et al., 2019; Song et al., 2003; Weller et al., 2016; Yang et al., 2009; Zhai et al., 2011a). The eclogite samples consist of garnet, omphacite, epidote, amphibole, zoisite, symplectite along with minor phengite, quartz, rutile, and rare apatite, ilmenite, and titanite as accessory minerals. Since the eclogite samples have suffered retrograde metamorphism, we assume that is largely composed of garnet and omphacite plus slight epidote before retrograde metamorphism. The accessory phases observed in natural eclogite are excluded because of their minimal abundance of less than 5%. Based on the mineral composition data of exposed eclogite in Tibet (Fig. S3) (e.g. Cheng et al., 2015; Dong et al., 2018; Huang et al., 2015; Jin et al., 2019; Li et al., 2017; Yang et al., 2014; Zhai et al., 2011b, 2011a), the components of eclogite are 50 vol. % garnet + 45 vol. % omphacite + 5 vol. % epidote (parameterized as a value out of 100) using the normal distribution.

We take into account two different delamination modes, namely, delamination caused by the separation of the Neo-Tethyan slab (detachment of the subducted Neo-Tethyan oceanic slab) in the

https://doi.org/10.5194/se-2021-115
Preprint. Discussion started: 29 September 2021

Paleozoic and convective removal of the lower crust of the subducted Indian continent beneath the Lhasa terrane during the Cenozoic. The temperature and pressure conditions of exposed eclogites in the Paleozoic and Cenozoic are somewhat consistent with the geothermal lines provided by previous studies (Fig. 4). The two different delamination modes reflect relatively cold geotherms and hot geotherms, respectively. Therefore, these geothermal lines are used in our models. The thermal EoS parameters of eclogitic garnet, omphacite, and epidote are derived through the HT-BM3-EoS shown in supporting information Table S2.

5.1 The density of main minerals for eclogite along the geothermal profile in Tibet

Tibetan eclogite is mainly composed of garnet, and omphacite, with a few epidotes. As shown in Figure 2, the exposed minerals differ in composition. The specific composition of minerals constrains the density. Therefore, we refer to the thermoelastic parameters of Xu et al. (2019) and Nishihara et al. (2003) to depict the density distribution of different components (Fe content) of garnet and omphacite under Tibetan geothermal lines, respectively. The corresponding thermoelastic parameters can be seen in Table S3. The mineral compositions of previous studies are within the range of the Tibetan constituents collected in this study (Fig. 2).

The density distribution of minerals along with relatively cold Tibetan geothermal conditions is shown in Figure 5 (the results along with hot geotherms can be seen in supporting information Fig. S6). The result clearly shows that the density of garnet is linked with the iron content. The density of garnet ($Prp_{21}Alm_{47}Grs_{31}Sps_1$, with 47 mol. % almandine) in this study is higher than that of low-Fe garnet ($Prp_{28}Alm_{38}Grs_{33}Sps_1$, with 38 mol. % almandine) (Xu et al., 2019) by 2.25% but lower than that of high-Fe garnet ($Prp_{14}Alm_{62}Grs_{19}Adr_3Sps_2$, with 62 mol. % almandine) (Xu et al., 2019) by 3.74% at ~80 km (Fig. 5a). With increasing depth, the density of high-Fe garnet

https://doi.org/10.5194/se-2021-115
Preprint. Discussion started: 29 September 2021

increases by a larger amplitude. This discrepancy may be caused by its smaller degree of thermal expansion (2.56 (44)$\times 10^{-5}$ K^{-1}). Accordingly, the influence of pressure on the density is greater than that of temperature, which leads to faster increases in density with depth. The density of omphacite does not show obvious characteristics related to its composition. The density of omphacite ($Quad_{48}Jd_{45}Ae_7$, with 7 mol. % aegirine) in this study is lower than that of high-Fe omphacite ($Quad_{53}Jd_{27}Ae_{20}$, with 20 mol. % aegirine) (Xu et al., 2019), $Quad_{72}Jd_{28}$ (Nishihara et al., 2003), and $Quad_{57}Jd_{42}Ae_1$ (with 1 mol. % aegirine) (Xu et al., 2019) by 2.07%, 1.63%, and 0.99%, respectively, at ~80 km (Fig. 5b). The presence of iron in certain quantities does increase the density of omphacite, but the density of omphacite is also affected by other elements, such as calcium and magnesium. Moreover, thermal EoS parameters are also of vital importance to calculate the density. The relatively low thermal expansion of $Quad_{72}Jd_{28}$ (2.7 (3)$\times 10^{-5}$ K^{-1}) and $Quad_{57}Jd_{42}Ae_1$ (with 1 mol. % aegirine) (2.8 (3)$\times 10^{-5}$ K^{-1}) may further enhance the increasing rate of density with depth. It is worth noting that the densities of $Quad_{48}Jd_{45}Ae_7$ (with 7 mol. % aegirine) in this study and $Quad_{57}Jd_{42}Ae_1$ (with 1 mol. % aegirine) of Xu et al. (2019) are the same under ambient conditions but inconsistent under high-pressure and high-temperature conditions. Therefore, the K_{T0} and K_{T0}' of the two omphacites are somewhat consistent with each other, while the thermal expansion and $(\partial K_T/\partial T)_P$ are different. Collectively, the thermal EoS parameters are of the essence in the derivation of the mineral density.

5.2 The density of eclogite in Tibet

Eclogitized crust and lithospheric mantle may be potential factors causing delamination (Faccenda et al., 2009; Krystopowicz and Currie, 2013; Ueda et al., 2012). The density of eclogite and peridotite can provide new constraints to control the breakoff of the subducted slab and convective

https://doi.org/10.5194/se-2021-115
Preprint. Discussion started: 29 September 2021

removal of the lithosphere in the process of delamination. Therefore, we plot the density distribution of eclogite with different garnet contents and peridotite along the Paleozoic and Cenozoic Tibetan geotherms, as shown in Figure 6. In our model, the mineral composition of Tibetan eclogite is in the range of 40 vol. % garnet + 55 vol. % omphacite + 5 vol. % epidote to 60 vol. % garnet + 35 vol. % omphacite + 5 vol. % epidote based on the exposed eclogite in Tibet (the composition of epidote is only 5 vol. % default due to its low content in this study). The composition of surrounding peridotite consists of 70 vol. % olivine + 25 vol. % orthopyroxene + 3 vol. % clinopyroxene + 2 vol. % spinel (Konstantinovskaia et al., 2003; Yang et al., 2019; Zhao et al., 2021). The densities of eclogite and peridotite aggregates are obtained considering their arithmetic mean. The density of each mineral under a specific temperature and room pressure can be calculated by the following equations:

$$\rho(T,0)=\rho_0 \exp\left[-\int_{T_0}^{T'} \alpha(T)\mathrm{dT}\right] \tag{1}$$

$$\alpha(T)=\alpha_0+\alpha_1 T+\alpha_2 T^{-1}+\alpha_3 T^{-2} \tag{2}$$

where ρ (T, 0) and ρ_0 are the densities of specific and ambient temperatures, respectively. α (T) is the thermal expansion coefficient, which is a function of temperature. Here, we define α (T) to be a constant (Table S2). The relationship with pressure is obtained according to the third-order Birch-Murnaghan equation of state and Euler finite strain theory (Birch, 1947, 1978):

$$P=(3/2)\left(K_0+(T-T_0)(\partial K/\partial T)_P\right)\left[(V_{T0}/V)^{7/3}-(V_{T0}/V)^{5/3}\right]\left\{1+(3/4)(K_{T0}'-4)\left[(V_{T0}/V)^{2/3}-1\right]\right\} \tag{3}$$

where V_{T0}, K_{T0}, and K_{T0}' are the unit cell volume, bulk modulus, and its pressure derivative, respectively, V is the unit cell volume at high pressures, and $(\partial K_T/\partial T)_P$ is the temperature derivative of the bulk modulus. The densities of each mineral under specific temperature and

https://doi.org/10.5194/se-2021-115
Preprint. Discussion started: 29 September 2021

pressure conditions are derived by the following formula:

$$\rho(T,P) = \rho(T,0)V(P,T) \tag{4}$$

Most changes in the deep conditions of the Earth are progressing slowly, so there is adequate time for recrystallization to relieve the maximum stress point (Robertson, 1988; Skinner, 1966). Here, we assume that the elastic-plastic interaction among different minerals and possible deviations from hydrostatic conditions are ignored and the density of the eclogite aggregate can be obtained by the arithmetic mean as follows:

$$\overline{\rho} = \sum \lambda_i \rho_i (T,P) \tag{5}$$

where the subscript *i* denotes the *i*th mineral of the upper mantle, and λ is the proportion of each mineral.

The densities of Tibetan eclogite (with the garnet composition of $Prp_{21}Alm_{47}Grs_{31}Sps_1$, the omphacite composition of $Quad_{48}Jd_{45}Ae_7$, and the epidote composition of $Ca_{2.02}Fe_{0.75}Al_{2.32}Si_{0.16}(SiO_4)(Si_2O_7)O(OH)$) and peridotite (with the olivine composition of $Fo_{89.9}Fa_{10.1}$, the orthopyroxene composition of $En_{89.6}Fs_{9.7}Wo_{0.7}$, the clinopyroxene composition of $Quad_{88.5}Jd_{11.5}$, and the spinel composition of $(Mg_{0.790}Fe_{0.204}Ni_{0.005}Ti_{0.001})_{1.000}(Al_{0.821}Cr_{0.158}Fe_{0.021})_{2.002}O_4$) in this study along the Paleozoic geothermal line are shown in Figure 6a. The results show that the increase in garnet has a profound influence on the density of eclogite. For every 10% increase in garnet, the density of eclogite increases by ~1.7%. The garnet content in Tibetan eclogite is estimated to be 40 vol. %-60 vol. % (Fig. S7). The densities of this part of eclogite are 3.55-3.67 g/cm^3, which is approximately 7.7%-11.5% more than that of peridotite (3.29 g/cm^3) at ~80 km. The density difference between eclogite and peridotite is 0.25 g/cm^3-0.38 g/cm^3 (Fig. 6b). At the same time, we also consider the

https://doi.org/10.5194/se-2021-115
Preprint. Discussion started: 29 September 2021

density of eclogite aggregates without epidote (Fig. S7). The results show that 5 vol. % epidote has little effect on the density of eclogite, especially eclogite with garnet contents of 50 vol. %-60 vol. %. To account for the role of iron, the density distributions of high-Fe ($Prp_{14}Alm_{62}Grs_{19}Adr_3Sps_2$ and $Quad_{53}Jd_{27}Ae_{20}$ and low-Fe eclogite ($Prp_{28}Alm_{38}Grs_{33}Sps_1$ and $Quad_{57}Jd_{42}Ae_1$) are plotted to better constrain the range of eclogite density (Fig. S9) (Xu et al., 2019). For high-Fe and low-Fe eclogites, the densities of eclogite increase by ~1.9% and ~1.4% for each 10% increase in garnet, respectively. The densities of eclogite are 3.64 g/cm^3-3.78 g/cm^3 for high-Fe content and 3.53 g/cm^3-3.63 g/cm^3 for low-Fe content at ~80 km. Furthermore, the densities of high-Fe and low-Fe eclogites are 10.6%-14.9% and 7.2%-10.3% higher than the surrounding peridotite, respectively. For a more straightforward comparison, taking eclogite containing 50 vol. % garnet as an example (Fig. S10), the densities of high-Fe eclogite, low-Fe eclogite, and Tibetan eclogite at ~80 km are 3.71 g/cm^3, 3.58 g/cm^3, and 3.61 g/cm^3, respectively. An increase in the iron content can substantially increase the density of eclogite, although it will be constrained by the thermal EoS parameters of minerals.

Similarly, we also discuss the density profile along the Cenozoic geothermal line, which can be seen in supporting information Text S3. In any case, the density difference caused by eclogite may be one of the prominent factors instigating the delamination process.

5.3 Influence of the degree of eclogitization on the density of the subducted slab

Eclogite in the mantle, which is believed to be 5%-10% denser than peridotite (Garber et al., 2018), is responsible for the excess compositional density. Furthermore, some calculations propose that the degree of eclogitization of the subducted slab is a key factor in the delamination process (Matchette-Downes et al., 2019). To investigate the influence of the degree of

https://doi.org/10.5194/se-2021-115
Preprint. Discussion started: 29 September 2021

eclogitization in the delamination process, we plot the density variations with different mineral compositions under different degrees of eclogitization (Fig. 7). We consider eclogitization in the lithospheric mantle of the subducted slab. In our preferred model, the 7-km thick subducted oceanic crust becomes eclogite, while the lithospheric mantle constrains a different amount of eclogite. Since the subducted Indian oceanic slab might be fragmented into several pieces, the longitudinal size of the fractured slab is postulated to be 60 km (Peng et al., 2016). Our estimated average density of the fragmented slab with various degrees of eclogitization is shown in Figure 7a. The results clearly show that the density increases monotonically with the garnet content and the degree of eclogitization. The garnet content is of profound importance to the density of eclogite. The higher the proportion of garnet is, the greater the density increases with increasing degrees of eclogitization. The garnet content in Tibetan eclogite is estimated to be between 40-60 vol. %. Taking garnet with an average volume percentage of 50 vol. % in Tibetan eclogite as an example, the density of eclogitized subducted slabs ranges from 3.37 g/cm^3 with 10% eclogitization to 3.61 g/cm^3 with 100 vol. % eclogitization. For a garnet content of 50 vol.%, the density increases by 0.026 g/cm^3 per 10 vol. % increase in the degree of eclogitization. The density will increase with increasing garnet contents, from 0.004 g/cm^3 for 10 vol. % to 0.048 g/cm^3 for 90 vol. %. The densities of high-Fe and low-Fe eclogitized fragmented slabs are also shown in Figure S11. The high-Fe content shows that the density variation increases with the degree of eclogitization from 0.007 g/cm^3 for 10 vol. % to 0.064 g/cm^3 for 90 vol. % garnet, while the low-Fe content shows a density change from 0.004 g/cm^3 for 10 vol. % garnet to 0.045 g/cm^3 for 90 vol. % garnet.

5.4 Delamination in Tibet

https://doi.org/10.5194/se-2021-115
Preprint. Discussion started: 29 September 2021

The development of delamination is associated with the instability of the lower crust and the mantle lithosphere. The eclogitization of the subducted slab and lower crust plays a vital role in the process of delamination due to the high density of eclogite (Anderson, 2005; Lee et al., 2011), which makes the formation denser than the surrounding mantle lithosphere and provides critical negative buoyancy (Göğüş and Ueda, 2018; Krystopowicz and Currie, 2013). The densities of the eclogitic lower crust and mantle lithosphere during slab subduction and convective removal are sufficiently higher than that of the asthenosphere and are good candidates for the initiation of destabilization.

5.4.1 Subducted slab breakoff

A series of collisional breakoff events is proposed to have occurred throughout 60-45 Ma in Tibet (Chung et al., 2005, 2009; Ma et al., 2014; Zhu et al., 2015). The formation of eclogite presumably kick-starts slab breakoff during the subduction of the Indian oceanic plate underthrust below the southern margin of Tibet. The subducted Indian oceanic slab fragmented into several pieces, due to what has been identified as a high-velocity anomaly (Peng et al., 2016; Razi et al., 2014; Shi et al., 2020b). The seismological evidence of high density (Hetényi et al., 2007), high V_P (Schulte-Pelkum et al., 2005), and low longitudinal/transverse (V_P/V_S) ratios (Wittlinger et al., 2009) further confirms that there may be variable degrees of eclogitization beneath Tibet. Figure 7 shows the density profile of subducted slabs with different garnet compositions, different degrees of eclogitization, and variable densities compared with the surrounding peridotite. An increasing degree of eclogitization and an enhanced garnet content in eclogite increases the density difference between the slab and the surrounding peridotite. Previous studies have made preliminary estimates of the average density from the isostatic balance and geoid anomalies, and postulated that the

https://doi.org/10.5194/se-2021-115
Preprint. Discussion started: 29 September 2021

density excess could be between 0-0.19 g/cm^3 (Matchette-Downes et al., 2019). For Tibetan eclogite containing 40 vol. %-60 vol. % garnet, if the lithospheric mantle is a mixture of peridotite and eclogite with a density anomaly of 0.19 g/cm^3, our model requires a range of 37%-64% degrees of eclogitization. If the eclogite is high-Fe, only a 30%-48% degree of eclogitization is needed to produce the density difference (Fig. S11), while an eclogitization degree is in the range of 49%-74% is needed for the low-Fe eclogite. However, some seismological data show that the crust or lithospheric mantle being only ~30% eclogitized might cause gravitational instability in Tibet (Matchette-Downes et al., 2019; Shi et al., 2020a), which is lower than our estimation. Our results clearly show that density excess is closely linked with garnet content and eclogitization degree. If eclogite has a high garnet content, a relatively low degree of eclogitization could instigate the delamination of slab breakoff.

On the other hand, the presence of a weak lower crust and a vertical conduit to accommodate asthenosphere influx is also necessary for the delamination process. The weak layer between the residual crustal and downward peeling lithosphere layer (and/or lower crust) (Göğüş and Ueda, 2018) could promote the initiation and propagation of delamination. Therefore, very high temperatures and relatively low lower-crustal viscosities are also other controlling factors of delamination (Göğüş and Pysklywec, 2008; Morency, 2004; Valera et al., 2011). Here, we assume that the length of the fractured slab is 60 km, which drops 80 km over 45 Ma and that the viscosity of the asthenosphere is $5*10^{20}$ Pa·S (Wang et al., 2019). By using Stokes' Law (Supporting Information Text S4), ignoring the thermal disturbance, and assuming the most ideal conditions, the density difference caused by eclogite needs to be at least 0.14 g/cm^3 to produce such delamination. The result is close to those discussed above in gravity anomalies.

In particular, the presence of eclogite with a greater abundance of garnet, a higher-Fe content, and a greater degree of eclogitization would instigate the delamination process of slab breakoff.

5.4.2 Removal of the eclogitized lower crust

The thickened lower crust undergoes “convective removal” due to gravitational instability, which is another type of delamination that occurred in Tibet from 25 Ma to 0 Ma (Chung et al., 2005; Nomade et al., 2004). The convective removal of the lithosphere during delamination corresponds to higher temperature conditions (Craig et al., 2020). In this circumstance, the density of Tibetan eclogite is 7.6%-11.6% denser than the surrounding peridotite at ~60 km (Fig. 6b), which is analogous to the results in the case of subducted slab detachment. This result is also in ample agreement with the result obtained by Garber et al. (2018), which noted that eclogite is 5%-10% denser than peridotite. The density difference between eclogite and peridotite is 0.24 g/cm^3-0.37 g/cm^3 with 40 vol. %-60 vol. % garnet in Tibet (Fig. 6d). During this stage, it is believed that delamination of the thickened, eclogitized lower crust has occurred. Similarly, Stokes’ law can be used considering ideal conditions without any thermal disturbance. If the falling block is assumed to be approximately 30 km in the longitudinal direction and the viscosity of the asthenosphere is $5*10^{20}$ Pa·S, the falling block can drop by 75-115 km within 25 Ma. For eclogite with a high-Fe content, a density difference of 0.35 g/cm^3-0.50 g/cm^3 makes the fragmented block capable of falling 105-155 km, while the density difference of 0.24 g/cm^3-0.33 g/cm^3 with a low-Fe content makes the block able to fall 75-102 km (Fig. S12). The fragmented block with a high-Fe content can fall a larger distance at the same time, indicating that the high-Fe content is more likely to promote the occurrence of delamination. This result is consistent with the high-velocity anomalous blocks identified at 100-200 km by seismic tomography (Peng et al., 2016; Shi et al.,

https://doi.org/10.5194/se-2021-115
Preprint. Discussion started: 29 September 2021

2016, 2020a).

In summary, density contrasts can provide a stimulus for the initiation of instability. It is accepted that eclogite with a high garnet content and a high Fe content and a high proportion of eclogite in the lithospheric mantle may have strongly promoted delamination during the process of India-Asia collision from the perspective of density.

6. Conclusion

The *P-V-T* EoS of the main minerals of eclogite is combined with its mineral composition and the geothermal line to derive the density of Tibetan eclogite in this study. We offer a new perspective by obtaining the thermal EoS for the main minerals of eclogite in a single experiment. The thermal EoS parameters of the main minerals of eclogite are derived by fitting the *P-V-T* data to the HT-BM-EoS. The density of minerals along the Tibetan geotherm shows that the density is closely related to its composition and thermal EoS parameters. Increasing iron contents increase the density of minerals, but if the molecular masses of two minerals are similar, the thermal EoS parameters play a pivotal role. The garnet content profoundly increases the density of eclogite. For every 10 vol. % increase in garnet, the density of eclogite increases by approximately 1.7%. The density of Tibetan eclogite is approximately 7-11% denser than that of the surrounding peridotite. An increasing proportion of garnet, Fe content, and degree of eclogitization enhance the density difference to facilitate the delamination process. For Tibetan eclogite containing 40-60 vol. % garnet, 37-64% degrees of eclogitization can produce the same density difference as obtained by the isostatic balance and the geoid anomaly. According to a rough calculation, the fragmented block will fall 75-155 km. A high-Fe content is more likely to promote delamination. Eclogite is a

https://doi.org/10.5194/se-2021-115
Preprint. Discussion started: 29 September 2021

good candidate for the initiation of instability and may be more susceptible to inducing the breakoff of the subducted slab or the gravitational removal of the lower crust during the process of the India-Asia collision.

Data availability

All the data presented in this paper are available upon request.

Author contributions

All authors contributed to the preparation and revision of the manuscript. Z. Ye: Data curation, Investigation, Formal analysis, Writing-original draft, Writing-review & editing. D. Fan: Investigation, Conceptualization, Supervision, Methodology, Funding acquisition, Writing-review & editing. B. Li: Data curation, Writing-review & editing. Q. Tang: Software, Validation, Writing-review & editing. J. Xu: Investigation, Supervision, Writing-review & editing. D. Zhang: Formal analysis, Writing-review & editing. W. Zhou: Investigation, Conceptualization, Supervision, Writing-review & editing.

Competing interests

The authors declare that they have no conflict of interest.

Disclaimer

Publisher's note: Copernicus Publications remains neutral with regard to jurisdictional claims in published maps and institutional affiliations.

Acknowledgments

This project was funded by the National Natural Science Foundation of China (Grant Nos. 42172048, U2032118 and 41802043), the Youth Innovation Promotion Association CAS (Dawei Fan, 2018434), the Chinese Academy of Sciences "Light of West China" Program (2019), the Guizhou Provincial Science and Technology Projects (QKHJC-ZK[2021]ZD042), and the Innovation and Entrepreneurship Funding of High-Level Overseas Talents of Guizhou Province (Dawei Fan, [2019] 10).

Supplementary Information. The supplementary information describes the density profile of garnet at high temperature, density profile along Cenozoic geothermal line, data of unit-cell parameters of eclogite minerals, thermal EoS parameters of this study and previous researches, figures of Eulerian finite stain-normalized pressure (F_E -f_E), isothermal bulk modulus (K_{T0}) and its pressure derivative (K_{T0}') plot of garnet and omphacite, normal distribution of eclogite minerals, density evolution of minerals, and density profile of different Fe-content eclogite.

References:

Anderson, D. L.: Large Igneous Provinces, Delamination, and Fertile Mantle, Elements, 1(5), 271–275, doi:10.2113/gselements.1.5.271, 2005.

Angel, R. J., Alvaro, M. and Gonzalez-Platas, J.: EosFit7c and a Fortran module (library) for equation of state calculations, Zeitschrift für Krist. - Cryst. Mater., 229(5), doi:10.1515/zkri-2013-1711, 2014.

Arimoto, T., Gréaux, S., Irifune, T., Zhou, C. and Higo, Y.: Sound velocities of $Fe_3Al_2Si_3O_{12}$ almandine up to 19 GPa and 1700 K, Phys. Earth Planet. Inter., 246, 1–8, doi:10.1016/j.pepi.2015.06.004, 2015.

Bajolet, F., Galeano, J., Funiciello, F., Moroni, M., Negredo, A.-M. and Faccenna, C.: Continental delamination: Insights from laboratory models, Geochemistry, Geophys. Geosystems, 13(2), doi:10.1029/2011GC003896, 2012.

Beyer, C., Kurnosov, A. V., Ballaran, T. B. and Frost, D. J.: High-pressure and high-temperature single-crystal X-ray diffraction of complex garnet solid solutions up to 16 GPa and 823 K, Phys. Chem. Miner., 48(4), 17, doi:10.1007/s00269-021-01139-5, 2021.

Birch, F.: Finite Elastic Strain of Cubic Crystals, Phys. Rev., 71(11), 809–824, doi:10.1103/PhysRev.71.809, 1947.

Birch, F.: Finite strain isotherm and velocities for single-crystal and polycrystalline NaCl at high pressures and 300 K, J. Geophys. Res., 83(B3), 1257, doi:10.1029/JB083iB03p01257, 1978.

Bird, P.: Initiation of intracontinental subduction in the Himalaya, J. Geophys. Res. Solid Earth, 83(B10), 4975–4987, doi:10.1029/JB083iB10p04975, 1978.

Bird, P.: Continental delamination and the Colorado Plateau, J. Geophys. Res. Solid Earth, 84(B13), 7561–7571, doi:10.1029/JB084iB13p07561, 1979.

Burov, E. B. and Watts, A. B.: The long-term strength of continental lithosphere: "jelly sandwich" or "crème brûlée"?, GSA Today, 16(1), 4, doi:10.1130/1052-5173(2006)016<4:TLTSOC>2.0.CO;2, 2006.

Chan, G. H. N., Waters, D. J., Searle, M. P., Aitchison, J. C., Horstwood, M. S. A., Crowley, Q., Lo, C. H. and Chan, J. S. L.: Probing the basement of southern Tibet: evidence from crustal xenoliths entrained in a Miocene ultrapotassic dyke, J. Geol. Soc. London., 166(1), 45–52, doi:10.1144/0016-76492007-145, 2009.

https://doi.org/10.5194/se-2021-115
Preprint. Discussion started: 29 September 2021

Solid Earth Discussions

Chemenda, A. I., Burg, J. P. and Mattauer, M.: Evolutionary model of the Himalaya–Tibet system: geopoembased on new modelling, geological and geophysical data, Earth Planet. Sci. Lett., 174(3–4), 397–409, doi:10.1016/S0012-821X(99)00277-0, 2000.

Chen, W. and Tenzer, R.: The application of a gravimetric forward modelling of the lithospheric structure for an estimate of the average density of the upper asthenosphere, Geod. Geodyn., 10(4), 265–275, doi:10.1016/j.geog.2019.04.003, 2019.

Cheng, H., Zhang, C., Vervoort, J. D., Lu, H., Wang, C. and Cao, D.: Zircon U–Pb and garnet Lu–Hf geochronology of eclogites from the Lhasa Block, Tibet, Lithos, 155, 341–359, doi:10.1016/j.lithos.2012.09.011, 2012.

Cheng, H., Liu, Y., Vervoort, J. D. and Lu, H.: Combined U-Pb, Lu-Hf, Sm-Nd and Ar-Ar multichronometric dating on the Bailang eclogite constrains the closure timing of the Paleo-Tethys Ocean in the Lhasa terrane, Tibet, Gondwana Res., 28(4), 1482–1499, doi:10.1016/j.gr.2014.09.017, 2015.

Chung, S.-L., Chu, M.-F., Zhang, Y., Xie, Y., Lo, C.-H., Lee, T.-Y., Lan, C.-Y., Li, X., Zhang, Q. and Wang, Y.: Tibetan tectonic evolution inferred from spatial and temporal variations in post-collisional magmatism, Earth-Science Rev., 68(3–4), 173–196, doi:10.1016/j.earscirev.2004.05.001, 2005.

Chung, S.-L., Chu, M.-F., Ji, J., O'Reilly, S. Y., Pearson, N. J., Liu, D., Lee, T.-Y. and Lo, C.-H.: The nature and timing of crustal thickening in Southern Tibet: Geochemical and zircon Hf isotopic constraints from postcollisional adakites, Tectonophysics, 477(1–2), 36–48, doi:10.1016/j.tecto.2009.08.008, 2009.

Conrad, C. P. and Molnar, P.: Convective instability of a boundary layer with temperature-and strain-rate-dependent viscosity in terms of "available buoyancy," Geophys. J. Int., 139(1), 51–68,

https://doi.org/10.5194/se-2021-115
Preprint. Discussion started: 29 September 2021

doi:10.1046/j.1365-246X.1999.00896.x, 1999.

Corrie, S. L., Kohn, M. J. and Vervoort, J. D.: Young eclogite from the Greater Himalayan Sequence, Arun Valley, eastern Nepal: P–T–t path and tectonic implications, Earth Planet. Sci. Lett., 289(3–4), 406–416, doi:10.1016/j.epsl.2009.11.029, 2010.

Craig, T. J., Kelemen, P. B., Hacker, B. R. and Copley, A.: Reconciling Geophysical and Petrological Estimates of the Thermal Structure of Southern Tibet, Geochemistry, Geophys. Geosystems, 21(8), doi:10.1029/2019GC008837, 2020.

DeCelles, P. G., Robinson, D. M. and Zandt, G.: Implications of shortening in the Himalayan fold-thrust belt for uplift of the Tibetan Plateau, Tectonics, 21(6), 12-1-12–25, doi:10.1029/2001TC001322, 2002.

DeCelles, P. G., Kapp, P., Quade, J. and Gehrels, G. E.: Oligocene-Miocene Kailas basin, southwestern Tibet: Record of postcollisional upper-plate extension in the Indus-Yarlung suture zone, Geol. Soc. Am. Bull., 123(7–8), 1337–1362, doi:10.1130/B30258.1, 2011.

Dera, P., Zhuravlev, K., Prakapenka, V., Rivers, M. L., Finkelstein, G. J., Grubor-Urosevic, O., Tschauner, O., Clark, S. M. and Downs, R. T.: High pressure single-crystal micro X-ray diffraction analysis with GSE_ADA/RSV software, High Press. Res., 33(3), 466–484, doi:10.1080/08957959.2013.806504, 2013.

Ding, L., Paul, K., Zhong, D. and Deng, W.: Cenozoic Volcanism in Tibet: Evidence for a Transition from Oceanic to Continental Subduction, J. Petrol., 44(10), 1833–1865, doi:10.1093/petrology/egg061, 2003.

Dong, Y.-L., Wang, B.-D., Zhao, W.-X., Yang, T.-N. and Xu, J.-F.: Discovery of eclogite in the Bangong Co–Nujiang ophiolitic mélange, central Tibet, and tectonic implications, Gondwana Res., 35, 115–123, doi:10.1016/j.gr.2016.03.010, 2016.

Dong, Y., Xie, C., Yu, Y., Wang, B., Li, L. and Zeng, X.: The discovery of Longyasongduo eclogite from Gongbujiangda County, Tibet, and its significance., Geol. Bull. Of China, 37(8), 2018.

Duesterhoeft, E., Bousquet, R., Wichura, H. and Oberhänsli, R.: Anorogenic plateau formation: The importance of density changes in the lithosphere, J. Geophys. Res. Solid Earth, 117(B7), doi:10.1029/2011JB009007, 2012.

Ehlers, T. A. and Poulsen, C. J.: Influence of Andean uplift on climate and paleoaltimetry estimates, Earth Planet. Sci. Lett., 281(3–4), 238–248, doi:10.1016/j.epsl.2009.02.026, 2009.

Elkins-Tanton, L. T.: Continental magmatism, volatile recycling, and a heterogeneous mantle caused by lithospheric gravitational instabilities, J. Geophys. Res., 112(B3), B03405, doi:10.1029/2005JB004072, 2007.

Faccenda, M., Minelli, G. and Gerya, T. V.: Coupled and decoupled regimes of continental collision: Numerical modeling, Earth Planet. Sci. Lett., 278(3–4), 337–349, doi:10.1016/j.epsl.2008.12.021, 2009.

Fan, D., Xu, J., Wei, S., Chen, Z. and Xie, H.: In-situ high-pressure synchrotron X-ray diffraction of natural epidote, Chin. J. High Press. Phys., 28, 257–261, doi:10.11858/gywlxb.2014.03.001, 2014.

Fei, Y., Ricolleau, A., Frank, M., Mibe, K., Shen, G. and Prakapenka, V.: Toward an internally consistent pressure scale, Proc. Natl. Acad. Sci., 104(22), 9182–9186, doi:10.1073/pnas.0609013104, 2007.

Finkelstein, G. J., Jackson, J. M., Sturhahn, W., Zhang, D., Alp, E. E. and Toellner, T. S.: Single-crystal equations of state of magnesiowüstite at high pressures, Am. Mineral., 102(8), 1709–1717, doi:10.2138/am-2017-5966, 2017.

https://doi.org/10.5194/se-2021-115
Preprint. Discussion started: 29 September 2021

Garber, J. M., Maurya, S., Hernandez, J., Duncan, M. S., Zeng, L., Zhang, H. L., Faul, U., McCammon, C., Montagner, J., Moresi, L., Romanowicz, B. A., Rudnick, R. L. and Stixrude, L.: Multidisciplinary Constraints on the Abundance of Diamond and Eclogite in the Cratonic Lithosphere, Geochemistry, Geophys. Geosystems, 19(7), 2062–2086, doi:10.1029/2018GC007534, 2018.

Gatta, G. D., Merlini, M., Lee, Y. and Poli, S.: Behavior of epidote at high pressure and high temperature: a powder diffraction study up to 10 GPa and 1200 K, Phys. Chem. Miner., 38(6), 419–428, doi:10.1007/s00269-010-0415-y, 2011.

Gerya, T. V., Yuen, D. A. and Maresch, W. V.: Thermomechanical modelling of slab detachment, Earth Planet. Sci. Lett., 226(1–2), 101–116, doi:10.1016/j.epsl.2004.07.022, 2004.

Göğüş, O. H. and Pysklywec, R. N.: Near-surface diagnostics of dripping or delaminating lithosphere, J. Geophys. Res., 113(B11), B11404, doi:10.1029/2007JB005123, 2008.

Göğüş, O. H. and Ueda, K.: Peeling back the lithosphere: Controlling parameters, surface expressions and the future directions in delamination modeling, J. Geodyn., 117(March), 21–40, doi:10.1016/j.jog.2018.03.003, 2018.

Gorczyk, W., Hobbs, B. and Gerya, T.: Initiation of Rayleigh-Taylor instabilities in intra-cratonic settings, Tectonophysics, 514–517, 146–155, doi:10.1016/j.tecto.2011.10.016, 2012.

Gréaux, S. and Yamada, A.: P-V-T equation of state of $Mn_3Al_2Si_3O_{12}$ spessartine garnet, Phys. Chem. Miner., 41(2), 141–149, doi:10.1007/s00269-013-0632-2, 2014.

Guillot, S., Mahéo, G., de Sigoyer, J., Hattori, K. H. and Pêcher, A.: Tethyan and Indian subduction viewed from the Himalayan high- to ultrahigh-pressure metamorphic rocks, Tectonophysics, 451(1–4), 225–241, doi:10.1016/j.tecto.2007.11.059, 2008.

Hacker, B. R.: Hot and Dry Deep Crustal Xenoliths from Tibet, Science (80)., 287(5462), 2463–2466, doi:10.1126/science.287.5462.2463, 2000.

Hao, M., Zhang, J. S., Pierotti, C. E., Ren, Z. and Zhang, D.: High-Pressure Single-Crystal Elasticity and Thermal Equation of State of Omphacite and Their Implications for the Seismic Properties of Eclogite in the Earth's Interior, J. Geophys. Res. Solid Earth, 124(3), 2368–2377, doi:10.1029/2018JB016964, 2019.

He, Y., Li, S., Hoefs, J., Huang, F., Liu, S.-A. and Hou, Z.: Post-collisional granitoids from the Dabie orogen: New evidence for partial melting of a thickened continental crust, Geochim. Cosmochim. Acta, 75(13), 3815–3838, doi:10.1016/j.gca.2011.04.011, 2011.

Hetényi, G., Cattin, R., Brunet, F., Bollinger, L., Vergne, J., Nábělek, J. L. and Diament, M.: Density distribution of the India plate beneath the Tibetan plateau: Geophysical and petrological constraints on the kinetics of lower-crustal eclogitization, Earth Planet. Sci. Lett., 264(1–2), 226–244, doi:10.1016/j.epsl.2007.09.036, 2007.

Hodges, K. V., Hurtado, J. M. and Whipple, K. X.: Southward extrusion of Tibetan crust and its effect on Himalayan tectonics, Tectonics, 20(6), 799–809, doi:10.1029/2001TC001281, 2001.

Holland, T. J. B., Redfern, S. A. T. and Pawley, A. R.: Volume behavior of hydrous minerals at high pressure and temperature; II, Compressibilities of lawsonite, zoisite, clinozoisite, and epidote, Am. Mineral., 81(3–4), 341–348, doi:10.2138/am-1996-3-408, 1996.

Hou, Z.-Q., Gao, Y.-F., Qu, X.-M., Rui, Z.-Y. and Mo, X.-X.: Origin of adakitic intrusives generated during mid-Miocene east–west extension in southern Tibet, Earth Planet. Sci. Lett., 220(1–2), 139–155, doi:10.1016/S0012-821X(04)00007-X, 2004.

Houseman, G. and McKenzie, D. P.: Numerical experiments on the onset of convective instability in the Earth's mantle, Geophys. J. Int., 68(1), 133–164, doi:10.1111/j.1365-246X.1982.tb06966.x, 1982.

https://doi.org/10.5194/se-2021-115
Preprint. Discussion started: 29 September 2021

Houseman, G. A., McKenzie, D. P. and Molnar, P.: Convective instability of a thickened boundary layer and its relevance for the thermal evolution of continental convergent belts, J. Geophys. Res. Solid Earth, 86(B7), 6115–6132, doi:10.1029/JB086iB07p06115, 1981.

Huang, J., Tian, Z. Z., Zhang, C., Yang, J. J. and Chen, M.: Metamorphic evolution of Sumdo eclogite in Lhasa Block of the Tibetan Plateau: Phase equilibrium in NCKMnFMASHTO System, Geol. China, 42(5), 1559–1571, 2015.

Husson, L., Bernet, M., Guillot, S., Huyghe, P., Mugnier, J.-L., Replumaz, A., Robert, X. and Van der Beek, P.: Dynamic ups and downs of the Himalaya, Geology, 42(10), 839–842, doi:10.1130/G36049.1, 2014.

Jiang, F., Speziale, S. and Duffy, T. S.: Single-crystal elasticity of grossular- and almandine-rich garnets to 11 GPa by Brillouin scattering, J. Geophys. Res. Solid Earth, 109(B10), doi:10.1029/2004JB003081, 2004.

Jiang, Y.-H., Liu, Z., Jia, R.-Y., Liao, S.-Y., Zhou, Q. and Zhao, P.: Miocene potassic granite–syenite association in western Tibetan Plateau: Implications for shoshonitic and high Ba–Sr granite genesis, Lithos, 134–135, 146–162, doi:10.1016/j.lithos.2011.12.012, 2012.

Jiménez-Munt, I., Fernàndez, M., Vergés, J. and Platt, J. P.: Lithosphere structure underneath the Tibetan Plateau inferred from elevation, gravity and geoid anomalies, Earth Planet. Sci. Lett., 267(1–2), 276–289, doi:10.1016/j.epsl.2007.11.045, 2008.

Jin, X., Zhang, Y.-X., Zhou, X.-Y., Zhang, K.-J., Li, Z.-W., Khalid, S. Bin, Hu, J.-C., Lu, L. and Sun, W.-D.: Protoliths and tectonic implications of the newly discovered Triassic Baqing eclogites, central Tibet: Evidence from geochemistry, Sr Nd isotopes and geochronology, Gondwana Res., 69, 144–162, doi:10.1016/j.gr.2018.12.011, 2019.

Kind, R.: Seismic Images of Crust and Upper Mantle Beneath Tibet: Evidence for Eurasian Plate Subduction, Science (80)., 298(5596), 1219–1221, doi:10.1126/science.1078115, 2002.

Klotz, S., Chervin, J.-C., Munsch, P. and Le Marchand, G.: Hydrostatic limits of 11 pressure transmitting media, J. Phys. D. Appl. Phys., 42(7), 075413, doi:10.1088/0022-3727/42/7/075413, 2009.

Kohn, M. J. and Parkinson, C. D.: Petrologic case for Eocene slab breakoff during the Indo-Asian collision, Geology, 30(7), 591, doi:10.1130/0091-7613(2002)030<0591:PCFESB>2.0.CO;2, 2002.

Konstantinovskaia, E. A., Brunel, M. and Malavieille, J.: Discovery of the Paleo-Tethys residual peridotites along the Anyemaqen–KunLun suture zone (North Tibet), Comptes Rendus Geosci., 335(8), 709–719, doi:10.1016/S1631-0713(03)00118-4, 2003.

Krystopowicz, N. J. and Currie, C. A.: Crustal eclogitization and lithosphere delamination in orogens, Earth Planet. Sci. Lett., 361, 195–207, doi:10.1016/j.epsl.2012.09.056, 2013.

Lee, C.-T. A., Luffi, P. and Chin, E. J.: Building and Destroying Continental Mantle, Annu. Rev. Earth Planet. Sci., 39(1), 59–90, doi:10.1146/annurev-earth-040610-133505, 2011.

Lee, H.-Y., Chung, S.-L., Lo, C.-H., Ji, J., Lee, T.-Y., Qian, Q. and Zhang, Q.: Eocene Neotethyan slab breakoff in southern Tibet inferred from the Linzizong volcanic record, Tectonophysics, 477(1–2), 20–35, doi:10.1016/j.tecto.2009.02.031, 2009.

Leech, M., Sing, S., Jain, A., Klemperer, S. and Manickavasagam, R.: The onset of India–Asia continental collision: Early, steep subduction required by the timing of UHP metamorphism in the western Himalaya, Earth Planet. Sci. Lett., 234(1–2), 83–97, doi:10.1016/j.epsl.2005.02.038, 2005.

Levin, L. E.: Structure of the thermal lithosphere and asthenosphere beneath oceans and continents, Geotectonics, 40(5), 357–366, doi:10.1134/S0016852106050037, 2006.

Li, B., Xu, J., Zhang, D., ZhilinYe, Huang, S., Fan, D., Zhou, W. and Xie, H.: Thermoelasticity and

https://doi.org/10.5194/se-2021-115
Preprint. Discussion started: 29 September 2021

stability of natural epidote at high pressure and high temperature: Implications for water transport during cold slab subduction, Geosci. Front., (January), doi:10.1016/j.gsf.2020.05.022, 2020.

Li, C., van der Hilst, R. D., Meltzer, A. S. and Engdahl, E. R.: Subduction of the Indian lithosphere beneath the Tibetan Plateau and Burma, Earth Planet. Sci. Lett., 274(1–2), 157–168, doi:10.1016/j.epsl.2008.07.016, 2008.

Li, H. and Fang, J.: Crustal and upper mantle density structure beneath the qinghai-tibet plateau and surrounding areas derived from EGM2008 geoid anomalies, ISPRS Int. J. Geo-Information, 6(1), 1–15, doi:10.3390/ijgi6010004, 2017.

Li, J. X., Fan, W. M., Zhang, L. Y., Ding, L., Sun, Y. L., Peng, T. P., Cai, F. L., Guan, Q. Y. and Sein, K.: Subduction of Indian continental lithosphere constrained by Eocene-Oligocene magmatism in northern Myanmar, Lithos, 348–349, 105211, doi:10.1016/j.lithos.2019.105211, 2019.

Li, P., Zhang, C., Liu, X., Shen, T., Qiu, T. and Yang, J.: The metamorphic processes of the Xindaduo eclogite in Tibet and its constrain on the evolutionary of the Paleo-Tethys subduction zone., Acta Petrol. Sin., 33(12), 2017.

Li, Z.-H., Liu, M. and Gerya, T.: Lithosphere delamination in continental collisional orogens: A systematic numerical study, J. Geophys. Res. Solid Earth, 121(7), 5186–5211, doi:10.1002/2016JB013106, 2016.

Liang, X., Chen, Y., Tian, X., Chen, Y. J., Ni, J., Gallegos, A., Klemperer, S. L., Wang, M., Xu, T., Sun, C., Si, S., Lan, H. and Teng, J.: 3D imaging of subducting and fragmenting Indian continental lithosphere beneath southern and central Tibet using body-wave finite-frequency tomography, Earth Planet. Sci. Lett., 443, 162–175, doi:10.1016/j.epsl.2016.03.029, 2016.

Liu, D., Wang, Z., Xiao, A., Zhang, Y., Li, W., Zu, Y., Yao, S., Lin, S. and Zhang, B.: Efficient Gene

https://doi.org/10.5194/se-2021-115
Preprint. Discussion started: 29 September 2021

Targeting in Zebrafish Mediated by a Zebrafish-Codon-Optimized Cas9 and Evaluation of Off-Targeting Effect, J. Genet. Genomics, 41(1), 43–46, doi:10.1016/j.jgg.2013.11.004, 2014.

Liu, H., Xiao, Y., Van den Kerkhof, A., Wang, Y., Zeng, L. and Guo, H.: Metamorphism and fluid evolution of the Sumdo eclogite, Tibet: Constraints from mineral chemistry, fluid inclusions and oxygen isotopes, J. Asian Earth Sci., 172(September 2018), 292–307, doi:10.1016/j.jseaes.2018.09.013, 2019.

Liu, Y., Santosh, M., Yuan, T., Li, H. and Li, T.: Reduction of buried oxidized oceanic crust during subduction, Gondwana Res., 32, 11–23, doi:10.1016/j.gr.2015.02.014, 2016.

Lu, C., Mao, Z., Lin, J., Zhuravlev, K. K., Tkachev, S. N. and Prakapenka, V. B.: Elasticity of single-crystal iron-bearing pyrope up to 20 GPa and 750 K, Earth Planet. Sci. Lett., 361, 134–142, doi:10.1016/j.epsl.2012.11.041, 2013.

Ma, L., Wang, B.-D., Jiang, Z.-Q., Wang, Q., Li, Z.-X., Wyman, D. A., Zhao, S.-R., Yang, J.-H., Gou, G.-N. and Guo, H.-F.: Petrogenesis of the Early Eocene adakitic rocks in the Napuri area, southern Lhasa: Partial melting of thickened lower crust during slab break-off and implications for crustal thickening in southern Tibet, Lithos, 196–197, 321–338, doi:10.1016/j.lithos.2014.02.011, 2014.

Ma, L., Wang, Q., Li, Z. X., Wyman, D. A., Yang, J. H., Jiang, Z. Q., Liu, Y. sheng, Gou, G. N. and Guo, H. F.: Subduction of Indian continent beneath southern Tibet in the latest Eocene (~ 35 Ma): Insights from the Quguosha gabbros in southern Lhasa block, Gondwana Res., 41, 77–92, doi:10.1016/j.gr.2016.02.005, 2017.

Matchette-Downes, H., van der Hilst, R. D., Gilligan, A. and Priestley, K.: Seismological constraints on the density, thickness and temperature of the lithospheric mantle in southwestern Tibet, Earth Planet. Sci. Lett., 524, 115719, doi:10.1016/j.epsl.2019.115719, 2019.

https://doi.org/10.5194/se-2021-115
Preprint. Discussion started: 29 September 2021

Meng, Y., Weidner, D. J. and Fei, Y.: Deviatoric stress in a quasi-hydrostatic diamond anvil cell: Effect on the volume-based pressure calibration, Geophys. Res. Lett., 20(12), 1147–1150, doi:10.1029/93GL01400, 1993.

Milani, S., Nestola, F., Alvaro, M., Pasqual, D., Mazzucchelli, M. L., Domeneghetti, M. C. and Geiger, C. A.: Diamond–garnet geobarometry: The role of garnet compressibility and expansivity, Lithos, 227, 140–147, doi:10.1016/j.lithos.2015.03.017, 2015.

Milani, S., Angel, R. J., Scandolo, L., Mazzucchelli, M. L., Ballaran, T. B., Klemme, S., Domeneghetti, M. C., Miletich, R., Scheidl, K. S., Derzsi, M., Tokár, K., Prencipe, M., Alvaro, M. and Nestola, F.: Thermo-elastic behavior of grossular garnet at high pressures and temperatures, Am. Mineral., 102(4), 851–859, doi:10.2138/am-2017-5855, 2017.

Miller, C., Schuster, R., Klotzli, U., Frank, W. and Purtscheller, F.: Post-Collisional Potassic and Ultrapotassic Magmatism in SW Tibet: Geochemical and Sr-Nd-Pb-O Isotopic Constraints for Mantle Source Characteristics and Petrogenesis, J. Petrol., 40(9), 1399–1424, doi:10.1093/petroj/40.9.1399, 1999.

Molnar, P., England, P. and Martinod, J.: Mantle dynamics, uplift of the Tibetan Plateau, and the Indian Monsoon, Rev. Geophys., 31(4), 357, doi:10.1029/93RG02030, 1993.

Morency, C.: Numerical simulations of the mantle lithosphere delamination, J. Geophys. Res., 109(B3), B03410, doi:10.1029/2003JB002414, 2004.

Nábělek, P. I. and Nábělek, J. L.: Thermal characteristics of the Main Himalaya Thrust and the Indian lower crust with implications for crustal rheology and partial melting in the Himalaya orogen, Earth Planet. Sci. Lett., 395, 116–123, doi:10.1016/j.epsl.2014.03.026, 2014.

Neil, E. A. and Houseman, G. A.: Rayleigh-Taylor instability of the upper mantle and its role in intraplate orogeny, Geophys. J. Int., 138(1), 89–107, doi:10.1046/j.1365-246x.1999.00841.x, 1999.

Nishihara, Y., Takahashi, E., Matsukage, K. and Kikegawa, T.: Thermal equation of state of omphacite, Am. Mineral., 88(1), 80–86, doi:10.2138/am-2003-0110, 2003.

Nomade, S., Renne, P. R., Mo, X., Zhao, Z. and Zhou, S.: Miocene volcanism in the Lhasa block, Tibet: spatial trends and geodynamic implications☆, Earth Planet. Sci. Lett., 221(1–4), 227–243, doi:10.1016/S0012-821X(04)00072-X, 2004.

Pandolfo, F., Nestola, F., Cámara, F. and Domeneghetti, M. C.: High-pressure behavior of space group P2/n omphacite, Am. Mineral., 97(2–3), 407–414, doi:10.2138/am.2012.3928, 2012a.

Pandolfo, F., Nestola, F., Cámara, F. and Domeneghetti, M. C.: New thermoelastic parameters of natural C2/c omphacite, Phys. Chem. Miner., 39(4), 295–304, doi:10.1007/s00269-012-0484-1, 2012b.

Panza, G. F., Brandmayr, E. and Romanelli, F.: A geophysical perspective on the lithosphere–asthenosphere system from Periadriatic to the Himalayan areas: the contribution of gravimetry, Rend. Lincei, 31(0123456789), 59–67, doi:10.1007/s12210-020-00892-z, 2020.

Pavese, A., Diella, V., Pischedda, V., Merli, M., Bocchio, R. and Mezouar, M.: Pressure-volume-temperature equation of state of andradite and grossular, by high-pressure and -temperature powder diffraction, Phys. Chem. Miner., 28(4), 242–248, doi:10.1007/s002690000144, 2001.

Peng, M., Jiang, M., Li, Z.-H., Xu, Z., Zhu, L., Chan, W., Chen, Y., Wang, Y., Yu, C., Lei, J., Zhang, L., Li, Q. and Xu, L.: Complex Indian subduction style with slab fragmentation beneath the Eastern Himalayan Syntaxis revealed by teleseismic P-wave tomography, Tectonophysics, 667, 77–86, doi:10.1016/j.tecto.2015.11.012, 2016.

Platt, J. P. and England, P. C.: Convective removal of lithosphere beneath mountain belts; thermal and

https://doi.org/10.5194/se-2021-115
Preprint. Discussion started: 29 September 2021

mechanical consequences, Am. J. Sci., 294(3), 307–336, doi:10.2475/ajs.294.3.307, 1994.

Qin, F., Wu, X., Wang, Y., Fan, D., Qin, S., Yang, K., Townsend, J. P. and Jacobsen, S. D.: High-pressure behavior of natural single-crystal epidote and clinozoisite up to 40 GPa, Phys. Chem. Miner., 43(9), 649–659, doi:10.1007/s00269-016-0824-7, 2016.

Razi, A. S., Levin, V., Roecker, S. W. and Huang, G. D.: Crustal and uppermost mantle structure beneath western Tibet using seismic traveltime tomography, Geochemistry, Geophys. Geosystems, 15(2), 434–452, doi:10.1002/2013GC005143, 2014.

Ren, Y. and Shen, Y.: Finite frequency tomography in southeastern Tibet: Evidence for the causal relationship between mantle lithosphere delamination and the north–south trending rifts, J. Geophys. Res., 113(B10), B10316, doi:10.1029/2008JB005615, 2008.

Rivers, M., Prakapenka, V., Kubo, A., Pullins, C., Holl, C. and Jacobsen, S.: The COMPRES/GSECARS gas-loading system for diamond anvil cells at the Advanced Photon Source, High Press. Res., 28(3), 273–292, doi:10.1080/08957950802333593, 2008.

Robertson, E. C.: Thermal properties of rocks., 1988.

Rowley, D. B.: Minimum Age of Initiation of Collision Between India and Asia North of Everest Based on the Subsidence History of the Zhepure Mountain Section, J. Geol., 106(2), 220–235, doi:10.1086/516018, 1998.

Schott, B. and Schmeling, H.: Delamination and detachment of a lithospheric root, Tectonophysics, 296(3–4), 225–247, doi:10.1016/S0040-1951(98)00154-1, 1998.

Schulte-Pelkum, V., Monsalve, G., Sheehan, A., Pandey, M. R., Sapkota, S., Bilham, R. and Wu, F.: Imaging the Indian subcontinent beneath the Himalaya, Nature, 435(7046), 1222–1225, doi:10.1038/nature03678, 2005.

https://doi.org/10.5194/se-2021-115
Preprint. Discussion started: 29 September 2021

Schurr, B., Rietbrock, A., Asch, G., Kind, R. and Oncken, O.: Evidence for lithospheric detachment in the central Andes from local earthquake tomography, Tectonophysics, 415(1–4), 203–223, doi:10.1016/j.tecto.2005.12.007, 2006.

Semprich, J., Simon, N. S. C. and Podladchikov, Y. Y.: Density variations in the thickened crust as a function of pressure, temperature, and composition, Int. J. Earth Sci., 99(7), 1487–1510, doi:10.1007/s00531-010-0557-7, 2010.

Shi, D., Wu, Z., Klemperer, S. L., Zhao, W., Xue, G. and Su, H.: Receiver function imaging of crustal suture, steep subduction, and mantle wedge in the eastern India–Tibet continental collision zone, Earth Planet. Sci. Lett., 414, 6–15, doi:10.1016/j.epsl.2014.12.055, 2015.

Shi, D., Zhao, W., Klemperer, S. L., Wu, Z., Mechie, J., Shi, J., Xue, G. and Su, H.: West–east transition from underplating to steep subduction in the India–Tibet collision zone revealed by receiver-function profiles, Earth Planet. Sci. Lett., 452, 171–177, doi:10.1016/j.epsl.2016.07.051, 2016.

Shi, D., Klemperer, S. L., Shi, J., Wu, Z. and Zhao, W.: Localized foundering of Indian lower crust in the India-Tibet collision zone, Proc. Natl. Acad. Sci. U. S. A., 117(40), 24742–24747, doi:10.1073/pnas.2000015117, 2020a.

Shi, Y.-N., Niu, F., Li, Z.-H. and Huangfu, P.: Craton destruction links to the interaction between subduction and mid-lithospheric discontinuity: Implications for the eastern North China Craton, Gondwana Res., 83, 49–62, doi:10.1016/j.gr.2020.01.016, 2020b.

Singh, A. and Kumar, M. R.: Seismic signatures of detached lithospheric fragments in the mantle beneath eastern Himalaya and southern Tibet, Earth Planet. Sci. Lett., 288(1–2), 279–290, doi:10.1016/j.epsl.2009.09.031, 2009.

Singh, H. and Mahatsente, R.: Lithospheric Structure of Eastern Tibetan Plateau from Terrestrial and

https://doi.org/10.5194/se-2021-115
Preprint. Discussion started: 29 September 2021

Solid Earth Discussions

Satellite Gravity Data Modeling: Implication for Asthenospheric Underplating, edited by S. Roeske, Lithosphere, 2020(1), doi:10.2113/2020/8897964, 2020.

Skinner, B. J.: Section 6: Thermal expansion, in Handbook of Physical Constants, pp. 75–96, Geological Society of America., 1966.

Sobolev, S. V. and Babeyko, A. Y.: What drives orogeny in the Andes?, Geology, 33(8), 617–620, doi:10.1130/G21557AR.1, 2005.

Song, S. G., Yang, J. S., Xu, Z. Q., Liou, J. G. and Shi, R. D.: Metamorphic evolution of the coesite-bearing ultrahigh-pressure terrane in the North Qaidam, Northern Tibet, NW China, J. Metamorph. Geol., 21(6), 631–644, doi:10.1046/j.1525-1314.2003.00469.x, 2003.

Sun, M., Tang, J. X., Chen, W., Ma, X. D., Qu, X. M., Song, Y., Li, X. Y. and Ding, J. S.: Process of lithospheric delamination beneath the Lhasa–Qiangtang collision orogen: Constraints from the geochronology and geochemistry of Late Cretaceous volcanic rocks in the Lhasa terrane, central Tibet, Lithos, 356–357, 105219, doi:10.1016/j.lithos.2019.105219, 2020.

Tang, Y., Qin, Y., Gong, X., Duan, Y., Chen, G., Yao, H., Liao, J., Liao, S., Wang, D. and Wang, B.: Discovery of eclogites in Jinsha River suture zone, Gonjo County, eastern Tibet and its restriction on Paleo-Tethyan evolution, China Geol., 3(1), 83–103, doi:10.31035/cg2020003, 2020.

Tian, S.-H., Yang, Z.-S., Hou, Z.-Q., Mo, X.-X., Hu, W.-J., Zhao, Y. and Zhao, X.-Y.: Subduction of the Indian lower crust beneath southern Tibet revealed by the post-collisional potassic and ultrapotassic rocks in SW Tibet, Gondwana Res., 41, 29–50, doi:10.1016/j.gr.2015.09.005, 2017.

Tilmann, F.: Seismic Imaging of the Downwelling Indian Lithosphere Beneath Central Tibet, Science (80)., 300(5624), 1424–1427, doi:10.1126/science.1082777, 2003.

Turner, S., Hawkesworth, C., Liu, J., Rogers, N., Kelley, S. and van Calsteren, P.: Timing of Tibetan uplift constrained by analysis of volcanic rocks, Nature, 364(6432), 50–54, doi:10.1038/364050a0, 1993.

Ueda, K., Gerya, T. V. and Burg, J.-P.: Delamination in collisional orogens: Thermomechanical modeling, J. Geophys. Res. Solid Earth, 117(B8), doi:10.1029/2012JB009144, 2012.

Valera, J. L., Negredo, A. M. and Jiménez-Munt, I.: Deep and near-surface consequences of root removal by asymmetric continental delamination, Tectonophysics, 502(1–2), 257–265, doi:10.1016/j.tecto.2010.04.002, 2011.

Wang, C., Zhao, X., Liu, Z., Lippert, P. C., Graham, S. A., Coe, R. S., Yi, H., Zhu, L., Liu, S. and Li, Y.: Constraints on the early uplift history of the Tibetan Plateau, Proc. Natl. Acad. Sci., 105(13), 4987–4992, doi:10.1073/pnas.0703595105, 2008.

Wang, C., Chen, W.-P. and Wang, L.-P.: Temperature beneath Tibet, Earth Planet. Sci. Lett., 375, 326–337, doi:10.1016/j.epsl.2013.05.052, 2013.

Wang, Q., Wyman, D.A., Li, Z.X., Sun, W., Chung, S.L., Vasconcelos, P.M., Zhang, Q.Y., Dong, H., Yu, Y.S., Pearson, N., Qiu, H.N., Zhu, T.X.: Eocene north–south trending dikes in central Tibet: new constraints on the timing of east. Earth and Planetary Science Letters 298 (1–2), 205–216, doi:10.1016/j.epsl.2010.07.046.

Wang, X., Holt, W. E. and Ghosh, A.: Joint modeling of lithosphere and mantle dynamics: Sensitivity to viscosities within the lithosphere, asthenosphere, transition zone, and D“ layers, Phys. Earth Planet. Inter., 293(March), 106263, doi:10.1016/j.pepi.2019.05.006, 2019.

Weller, O. M., St-Onge, M. R., Rayner, N., Waters, D. J., Searle, M. P. and Palin, R. M.: U–Pb zircon geochronology and phase equilibria modelling of a mafic eclogite from the Sumdo complex of south-east Tibet: Insights into prograde zircon growth and the assembly of the Tibetan plateau, Lithos,

https://doi.org/10.5194/se-2021-115
Preprint. Discussion started: 29 September 2021

262, 729–741, doi:10.1016/j.lithos.2016.06.005, 2016.

Williams, H., Turner, S., Kelley, S. and Harris, N.: Age and composition of dikes in Southern Tibet: New constraints on the timing of east-west extension and its relationship to postcollisional volcanism, Geology, 29(4), 339, doi:10.1130/0091-7613(2001)029<0339:AACODI>2.0.CO;2, 2001.

Wittlinger, G., Farra, V., Hetényi, G., Vergne, J. and Nábělek, J.: Seismic velocities in Southern Tibet lower crust: a receiver function approach for eclogite detection, Geophys. J. Int., 177(3), 1037–1049, doi:10.1111/j.1365-246X.2008.04084.x, 2009.

Xu, J., Zhang, D., Dera, P., Zhang, B. and Fan, D.: Experimental evidence for the survival of augite to transition zone depths, and implications for subduction zone dynamics, Am. Mineral., 102(7), 1516–1524, doi:10.2138/am-2017-5959, 2017.

Xu, J., Zhang, D., Fan, D., Zhang, J. S., Hu, Y., Guo, X., Dera, P. and Zhou, W.: Phase Transitions in Orthoenstatite and Subduction Zone Dynamics: Effects of Water and Transition Metal Ions, J. Geophys. Res. Solid Earth, 123(4), 2723–2737, doi:10.1002/2017JB015169, 2018.

Xu, J., Zhang, D., Fan, D., Dera, P. K., Shi, F. and Zhou, W.: Thermoelastic Properties of Eclogitic Garnets and Omphacites: Implications for Deep Subduction of Oceanic Crust and Density Anomalies in the Upper Mantle, Geophys. Res. Lett., 46(1), 179–188, doi:10.1029/2018GL081170, 2019.

Xu, J., Fan, D., Zhang, D., Li, B., Zhou, W. and Dera, P. K.: Investigation of the crystal structure of low water content hydrous olivine to 29.9 GPa: a high-pressure single-crystal X-ray diffraction study, Am. Mineral., doi:10.2138/am-2020-7444, 2020a.

Xu, J., Fan, D., Zhang, D., Guo, X., Zhou, W. and Dera, P. K.: Phase Transition of Enstatite-Ferrosilite Solid Solutions at High Pressure and High Temperature: Constraints on Metastable Orthopyroxene in Cold Subduction, Geophys. Res. Lett., 47(12), 1–10, doi:10.1029/2020GL087363, 2020b.

Xu, Y. G., Lan, J. B., Yang, Q. J., Huang, X. L. and Qiu, H. N.: Eocene break-off of the Neo-Tethyan slab as inferred from intraplate-type mafic dykes in the Gaoligong orogenic belt, eastern Tibet, Chem. Geol., 255(3–4), 439–453, doi:10.1016/j.chemgeo.2008.07.016, 2008.

Yang, J., Xu, Z., Li, Z., Xu, X., Li, T., Ren, Y., Li, H., Chen, S. and Robinson, P. T.: Discovery of an eclogite belt in the Lhasa block, Tibet: A new border for Paleo-Tethys?, J. Asian Earth Sci., 34(1), 76–89, doi:10.1016/j.jseaes.2008.04.001, 2009.

Yang, X., Zhang, L., Zhao, Z. and Zhu, D.: Metamorphic evolution of glaucophane eclogites from Sumdo，Lhasa block of Tibetan Plateau: Phase equilibria and metamorphic P-T path. Acta, Acta Petrol. Sin., 30(5), 2014.

Yang, Y., Abart, R., Yang, X., Shang, Y., Ntaflos, T. and Xu, B.: Seismic anisotropy in the Tibetan lithosphere inferred from mantle xenoliths, Earth Planet. Sci. Lett., 515, 260–270, doi:10.1016/j.epsl.2019.03.027, 2019.

Ye, Z., Fan, D., Tang, Q., Xu, J., Zhang, D. and Zhou, W.: Constraining the density evolution during destruction of the lithospheric mantle in the eastern North China Craton, Gondwana Res., 91, 18–30, doi:10.1016/j.gr.2020.12.001, 2021.

Zhai, Q., Zhang, R., Jahn, B., Li, C., Song, S. and Wang, J.: Triassic eclogites from central Qiangtang, northern Tibet, China: Petrology, geochronology and metamorphic P–T path, Lithos, 125(1–2), 173–189, doi:10.1016/j.lithos.2011.02.004, 2011a.

Zhai, Q., Jahn, B., Zhang, R., Wang, J. and Su, L.: Triassic Subduction of the Paleo-Tethys in northern Tibet, China: Evidence from the geochemical and isotopic characteristics of eclogites and blueschists of the Qiangtang Block, J. Asian Earth Sci., 42(6), 1356–1370, doi:10.1016/j.jseaes.2011.07.023, 2011b.

https://doi.org/10.5194/se-2021-115
Preprint. Discussion started: 29 September 2021

Zhang, C., Ma, C. and Holtz, F.: Origin of high-Mg adakitic magmatic enclaves from the Meichuan pluton, southern Dabie orogen (central China): Implications for delamination of the lower continental crust and melt-mantle interaction, Lithos, 119(3–4), 467–484, doi:10.1016/j.lithos.2010.08.001, 2010.

Zhang, D., Hu, Y. and Dera, P. K.: Compressional behavior of omphacite to 47 GPa, Phys. Chem. Miner., 43(10), 707–715, doi:10.1007/s00269-016-0827-4, 2016.

Zhang, D., Dera, P. K., Eng, P. J., Stubbs, J. E., Zhang, J. S., Prakapenka, V. B. and Rivers, M. L.: High Pressure Single Crystal Diffraction at PX^2, J. Vis. Exp., 2017(119), 1–9, doi:10.3791/54660, 2017a.

Zhang, L., Ng, Guo, Z., Zhang, M., Cheng, Z. and Sun, Y.: Post-collisional potassic magmatism in the eastern Lhasa terrane, South Tibet: Products of partial melting of mélanges in a continental subduction channel, Gondwana Res., 41, 9–28, doi:10.1016/j.gr.2015.11.007, 2017b.

Zhao, M.-S., Chen, Y.-X. and Zheng, Y.-F.: Geochemical evidence for forearc metasomatism of peridotite in the Xigaze ophiolite during subduction initiation in Neo-Tethyan Ocean, south to Tibet, Lithos, 380–381, 105896, doi:10.1016/j.lithos.2020.105896, 2021.

Zhao, S., Lai, S., Pei, X., Li, Z., Li, R., Qin, J., Zhu, R., Chen, Y., Wang, M., Pei, L., Liu, C. and Gao, F.: Neo-Tethyan evolution in southeastern extension of Tibet: Constraints from Early Paleocene to Early Eocene granitic rocks with associated enclaves in Tengchong Block, Lithos, 364–365, 105551, doi:10.1016/j.lithos.2020.105551, 2020.

Zhao, Z., Mo, X., Dilek, Y., Niu, Y., DePaolo, D. J., Robinson, P., Zhu, D., Sun, C., Dong, G. and Zhou, S.: Geochemical and Sr–Nd–Pb–O isotopic compositions of the post-collisional ultrapotassic magmatism in SW Tibet: Petrogenesis and implications for India intra-continental subduction beneath southern Tibet, Lithos, 113(1–2), 190–212, doi:10.1016/j.lithos.2009.02.004, 2009.

Zhu, D.-C., Zhao, Z.-D., Niu, Y., Mo, X.-X., Chung, S.-L., Hou, Z.-Q., Wang, L.-Q. and Wu, F.-Y.: The Lhasa Terrane: Record of a microcontinent and its histories of drift and growth, Earth Planet. Sci. Lett., 301(1–2), 241–255, doi:10.1016/j.epsl.2010.11.005, 2011.

Zhu, D.-C., Wang, Q., Zhao, Z.-D., Chung, S.-L., Cawood, P. A., Niu, Y., Liu, S.-A., Wu, F.-Y. and Mo, X.-X.: Magmatic record of India-Asia collision, Sci. Rep., 5(1), 14289, doi:10.1038/srep14289, 2015.

Zou, Y., Gréaux, S., Irifune, T., Whitaker, M. L., Shinmei, T. and Higo, Y.: Thermal equation of state of $Mg_3Al_2Si_3O_{12}$ pyrope garnet up to 19 GPa and 1700 K, Phys. Chem. Miner., 39(7), 589–598, doi:10.1007/s00269-012-0514-z, 2012.

https://doi.org/10.5194/se-2021-115
Preprint. Discussion started: 29 September 2021

Figure:

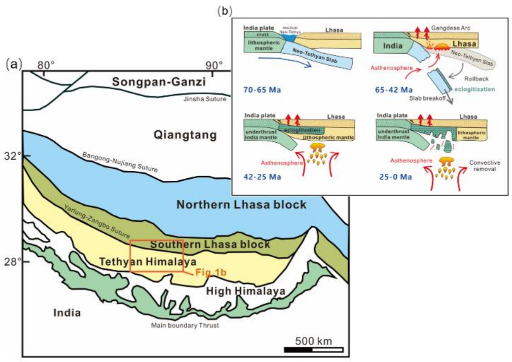

Figure 1. (a) Schematic geological map of the Tibetan Plateau (modified from Chung et al. 2005 and Wang et al. 2010). (b) Interpretive geological cartoon of India-Asia collision evolution . 70-65 Ma: The flat Neo-Tethyan oceanic slab subducts beneath Tibet with the closure of the Neo-Tethys Ocean. 65-42 Ma: The rollback of the Neo-Tethyan slab breaks off after densification by eclogitization. 42-25 Ma: The subduction of the Indian continent continued at a low subduction angle beneath the Lhasa terrane and was accompanied by heavy thermal perturbation. 25-0 Ma: The thickened eclogitic lower crust undergoes the “convective removal” of delamination due to gravitational instability.

https://doi.org/10.5194/se-2021-115
Preprint. Discussion started: 29 September 2021

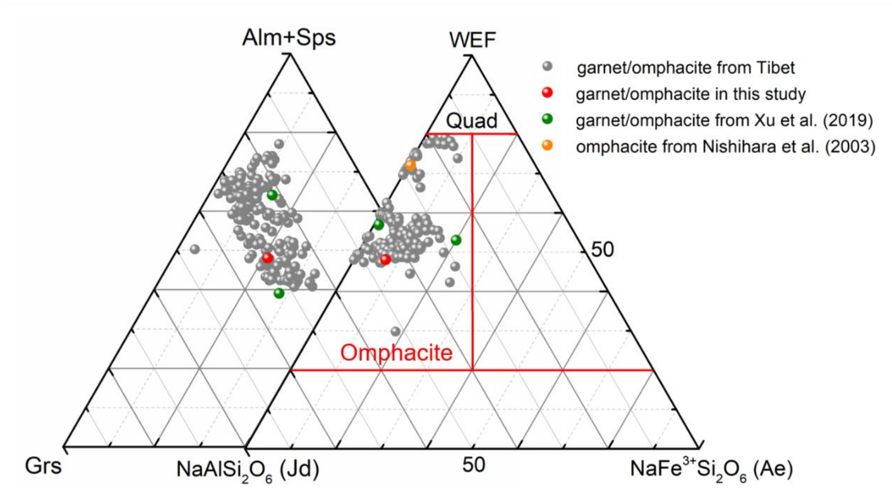

Figure 2. Composition of garnet and omphacite in eclogites from Tibet and this study. The gray solid circles represent the components of garnet and omphacite collected from previous studies in Tibet (e.g. Chan et al., 2009; Liu et al., 2019; Song et al., 2003; Weller et al., 2016; Yang et al., 2009; Zhai et al., 2011a). The green solid circles are garnet and omphacite with different Fe contents according to Xu et al. (2019). The orange solid circles are omphacite according to Nishihara et al. (2003). The red solid circles are the components of garnet and omphacite in this study. Prp = pyrope, Alm = almandine, Grs = grossular, Sps = spessartine, Quad = Ferrosilite + enstatite + wollastonite, Jd = jadeite, and Ae = aegirine.

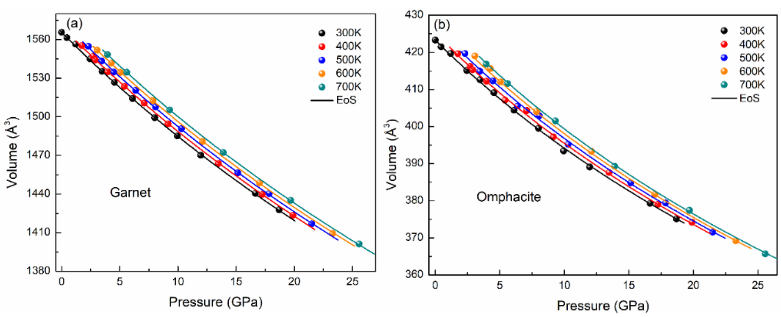

https://doi.org/10.5194/se-2021-115
Preprint. Discussion started: 29 September 2021

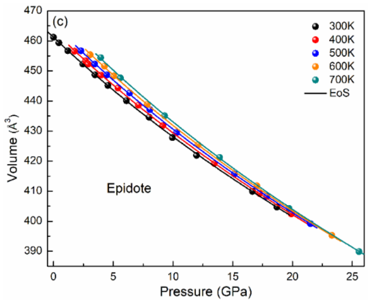

Figure 3. Pressure-volume-temperature relations of garnet (a), omphacite (b), and epidote (c). Isothermal compression curves are calculated by using the thermoelastic parameters obtained in this study.

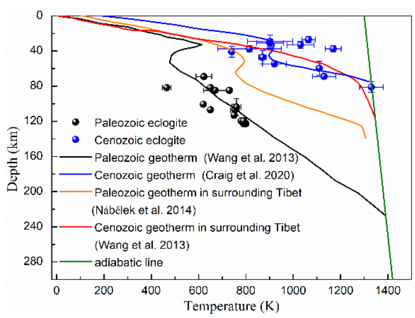

Figure 4. The geothermal lines of Tibet. The black line from Wang et al. (2013) represents the Paleozoic geotherm, which indicates relatively cold conditions. The delamination of the Neo-Tethyan slab breakoff accrues under such conditions. The orange line represents the geothermal line of surrounding Tibet during this period (Nábělek and Nábělek, 2014). The blue line represents the Cenozoic geotherm in Tibet (Craig et al., 2020), which indicates a relatively hot geotherm under the situation of convective removal. The red line represents the geothermal line of the surrounding Tibet in this situation (Wang et al., 2013). The green line is the adiabatic line. The black and blue solid circles correspond to the temperature and pressure conditions of exposed Tibetan eclogite in the Paleozoic and Cenozoic, respectively. The Paleozoic samples are referred

https://doi.org/10.5194/se-2021-115
Preprint. Discussion started: 29 September 2021

from (Cheng et al., 2012, 2015; Dong et al., 2016, 2018; Huang et al., 2015; Li et al., 2017; Liu et al., 2019; Tang et al., 2020; Weller et al., 2016; Yang et al., 2019, 2014) and the Cenozoic samples are referred from (Chan et al., 2009; Corrie et al., 2010; Hacker, 2000).

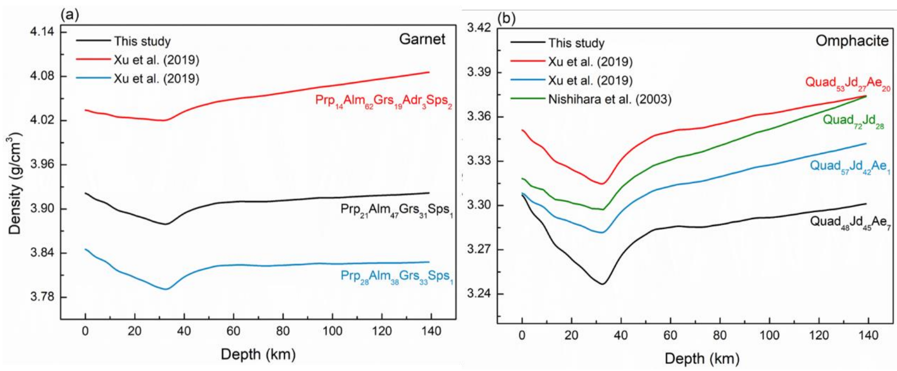

Figure 5. Density profiles of garnet (a) and omphacite (b) along with the cold Tibetan geothermal line (Wang et al., 2013). The garnets of $Prp_{21}Alm_{47}Grs_{31}Sps_1$ and $Prp_{28}Alm_{38}Grs_{33}Sps_1$ are from Xu et al. (2019). The omphacites of $Quad_{53}Jd_{27}Ae_{20}$ and $Quad_{57}Jd_{42}Ae_1$ are from Xu et al. (2019) and $Quad_{72}Jd_{28}$ is from Nishihara et al. (2003).

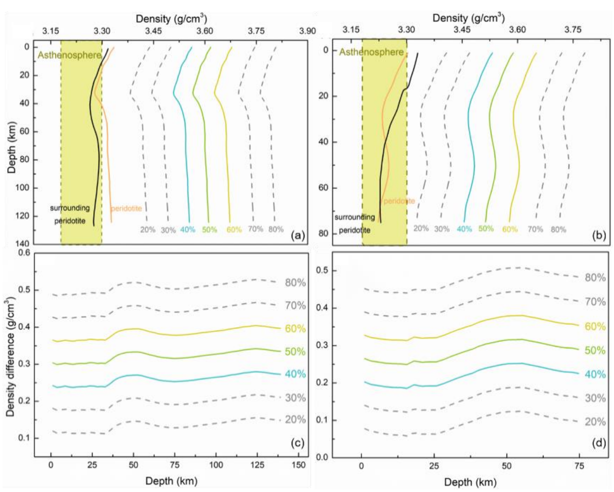

https://doi.org/10.5194/se-2021-115
Preprint. Discussion started: 29 September 2021

Figure 6. Density profiles of eclogite and peridotite assemblages ((a) and (b)) and density difference between eclogite and peridotite ((c) and (d)) in Tibet along the Paleozoic and Cenozoic geothermal lines under the conditions of Neo-Tethyan oceanic slab detachment (a) (Wang et al., 2013) and subduction of the Indian continental margin beneath the Lhasa terrane (b) (Craig et al., 2020). The percentage represents the content of garnet in eclogite, of which epidote accounts for 5 vol. % by default. The orange curve and black curve show the density profile of peridotite with a composition of 70 vol. % olivine + 25 vol. % orthopyroxene + 3 vol. % clinopyroxene + 2 vol. % spinel. The orange line shows the density of peridotite in the lithospheric mantle along the Paleozoic (a) (Wang et al., 2013) and Cenozoic (b) (Craig et al., 2020) geothermal lines, and the black curve indicates that the density of peridotite in the surrounding lithospheric mantle is along the Paleozoic (a) (Nábělek and Nábělek, 2014) and Cenozoic (b) (Wang et al., 2013) geothermal lines in Tibet. The shaded region is the density range of the asthenosphere (Chen and Tenzer, 2019; Levin, 2006; Panza et al., 2020; Singh and Mahatsente, 2020).

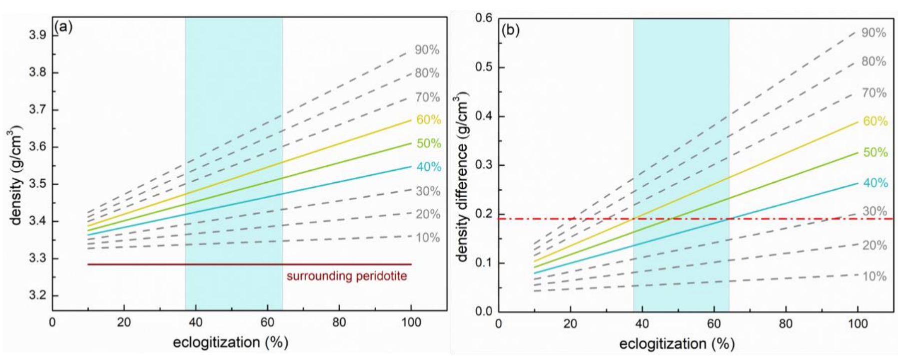

Figure 7. (a) The effect of eclogitization on the density of the subducted slab at ~80 km (2.6 GPa and 625 °C) along the Paleozoic geothermal line. The percentage on the right represents the content of garnet and the content of epidote is fixed at 5 vol. % by default. The content of garnets

https://doi.org/10.5194/se-2021-115
Preprint. Discussion started: 29 September 2021

in Tibet is between 40 vol. % and 60 vol. %. The density represents the average density of the subducted slab with the entire eclogitic ocean lower crust and partially eclogitized lithospheric mantle, where the degree of eclogitization refers to the lithospheric mantle. The rufous line represents the average density of surrounding peridotite in this study. The blue shading indicates the possible degree of eclogitization. (b) Density difference between eclogite with different degrees of eclogitization and surrounding peridotite. The red dashed solid line represents a density excess of 0.19 g/cm^3 from the isostatic balance and the geoid anomaly (Matchette-Downes et al., 2019).